Synthesis and Characterization of Chitosan/Cellulose-ZnO Nanocomposites for Bactericidal Applications

By

Melina L. Pérez-Altamar

A Thesis submitted for the requirements for the degree of

MASTER OF SCIENCE

In

Food Science and Technology

UNIVERSITY OF PUERTO RICO, MAYAGUEZ CAMPUS

2016

Approved by:

_____	_____
Oscar Perales – Pérez, Ph. D. President, Graduate Committee	Date
_____	_____
Félix R. Román, Ph. D. Member, Graduate Committee	Date
_____	_____
Lynette Orellana, Ph. D. Member, Graduate Committee	Date
_____	_____
Rafael Méndez, Ph. D. Representative of Graduate Studies	Date
_____	_____
Aixa Rivera, M.S. Chairperson of the Department	Date

ABSTRACT

The use of non-biodegradable plastics used in food packaging has generated a major environmental concern because of the waste generated. Besides, microbial contamination of food is a serious problem affecting the human health and the food industry. An alternative to face these concerns is the use of biopolymers-based nanocomposites, which are biodegradable and can be modified to provide protection against bacteria based on the tenability of their functional properties. On this basis, the present work focuses on the fabrication of chitosan/cellulose films hosting environmental friendly ZnO nanoparticles (NPs) as an attempt to produce nanocomposites with enhanced bactericidal capacity. Doping nanostructures is an efficient method of control and enhance their properties; it has been suggested that Mg doping influenced the bactericidal capacity of ZnO while enhancing UV blocking capacity. The solution casting method was used to fabricate the chitosan/cellulose blend films at various chitosan/cellulose w/w ratios. Highly monodisperse Mg doped ZnO nanoparticles were synthesized using Zinc acetate, Magnesium acetate and Triethylene glycol (TEG) via a modified Polyol route. The nanoparticles were inserted in the polymeric matrix at different weight percentages.

Optical properties of ZnO nanoparticles, pure and Mg-doped, were studied by UV–Vis Spectroscopy and Photoluminescence Spectroscopy (PL) techniques. The nanoparticles' size and morphology were determined by X- ray diffraction and Scanning Electron Microscopy (SEM). The chitosan/cellulose blend films and chitosan/cellulose- ZnO-Mg nanocomposites were characterized by Fourier Transform – Infrared spectroscopy (FTIR). The mechanical properties of produced bare and ZnO-bearing composites were

determined from stress-strain tests. The Standard Plate Count methods was used to evaluate the bactericidal properties of the pure and Mg-doped ZnO nanoparticles and chitosan/cellulose/ZnO-Mg nanocomposites against *Escherichia coli*.

The results reveal the formation of spherical nanoparticles of zinc oxide with a crystalline structure wurtzite and a crystal size in a range from 6 to 8 nm. The higher bactericidal capacity against *E. coli* was obtained for nanoparticles with a magnesium doping level of 0.5 at. %. In addition, all synthesized nanoparticles exhibited singlet oxygen generating capacity. Films made with chitosan and cellulose showed greater deformation when compared with the chitosan film. The tensile strength and water vapor permeability of the films increased with the insertion of the nanoparticles in the polymeric matrix. All nanocomposites formed by chitosan, cellulose and Mg-ZnO nanoparticles exhibited high bactericidal capacity against *E. coli*.

RESUMEN

El uso de plásticos no biodegradables usados en la industria de empaques de alimentos ha generado grandes preocupaciones ambientales, debido a los residuos generados. Además, la contaminación microbial de los alimentos es un serio problema que afecta la salud y a las industrias de alimentos. Una alternativa para enfrentar estas preocupaciones es el uso de nano compuestos fabricados con biopolímeros, los cuales son biodegradables y pueden ser modificados para proporcionar protección contra bacterias en base a sus propiedades funcionales. En base a esto, el presente trabajo se enfoca en la fabricación de películas de quitosano/celulosa con nanopartículas de óxido de zinc incorporadas, para producir un nanocompuesto con mejores capacidades bactericidas. El Dopaje de nanoestructuras es un método eficaz para controlar y mejorar sus propiedades; se ha sugerido que el dopaje con Mg influye en la capacidad bactericida del ZnO al tiempo que mejora la capacidad de bloquear los rayos UV. El método de "solution casting" fue usado para fabricar las películas de quitosano/celulosa a diferentes concentraciones de celulosa. Las nanopartículas de óxido de zinc puras y dopadas con magnesio fueron sintetizadas usando acetato de zinc, acetato de magnesio y tri-etilenglicol a través de una ruta "*poly-ol*" modificada. Las nanopartículas fueron insertadas en la matriz polimérica de quitosano/celulosa a diferentes porcentajes en peso. Las propiedades ópticas de las nanopartículas de ZnO puros y dopadas con Mg fueron estudiadas por técnicas de espectroscopía UV y fotoluminiscencia. El tamaño de las nanopartículas y la morfología se determinaron por difracción de rayos X y microscopía electrónica de barrido. Las películas de quitosano/celulosa con y sin nanopartículas fueron caracterizadas por espectroscopía infrarroja (FT-IR), y sus

propiedades mecánicas fueron determinadas por medio de ensayos de tensión. Las propiedades bactericidas de las nanopartículas puras y dopadas con Mg y del nanocompuesto fueron evaluadas contra *Escherichia coli* por medio del método de conteo de colonias.

Los resultados revelan la formación de nanopartículas esféricas de óxido de zinc con una estructura cristalina en la fase wurtzita, y con un tamaño del cristal en un rango entre 6 a 8 nm. La mayor capacidad bactericida contra *E. coli* se obtuvo para las nanopartículas con un nivel de dopaje de magnesio de 0.5 at. %. Además todas las nanopartículas sintetizadas exhibieron capacidad de generar oxigeno singlete.

Las películas fabricadas con quitosano y celulosa mostraron una mayor deformación al compararse con la película de quitosano. La inserción de nanopartículas en la matriz polimérica aumento la resistencia a la tensión y la permeabilidad al vapor de agua. Todos los nano-compuestos formados de quitosano, celulosa y nanopartículas de óxido de zinc exhibieron una alta capacidad bactericida contra *E. coli.*

God, thanks for the many blessings

Dedicated to my family…

In special my husband David and my son Juan David, for their unconditional support, inspiration and love.

To My father Jose, grandparents Miguel and Maritza, My sister Marly and my brother Jose Ricardo for their motivation and encouragement although in the distance.

To my mother Gloria… who always live in my heart.

ACKNOWLEDGMENTS

I'm sincerely grateful to the University of Puerto Rico at Mayaguez, especially the program of Food Science and Technology for been an important support in my professional development.

I am particularly grateful to the Nanotechnology Center (National Science Foundation grant HRD 0833112) and the UPRM Nanomaterials Processing Laboratory.

I want to thank my advisor Dr. Oscar Perales-Pérez for giving me an opportunity to work with him and for his direction and support throughout my research.

I would also like to thank my friends and coworkers at the Nanomaterials Processing Lab: Boris Renteria, Dra Yarilyn Cedeño, Ana Vega, Rebeca Caban, Milton Martinez, Myrna Reyes, Raquel Feliciano, Gina Montes, Angélica Quiñones, Miguel Santiago, Sujeily Soto, Jose Rodriguez, Hilary Marrero, Leomar Perez and Ivonnemary Rivera for their support and cooperation in my research.

TABLE OF CONTENTS

LIST OF FIGURES

LIST OF TABLES

CHAPTER I: INTRODUCTION

The use of non-biodegradable plastics in food packaging has generated a major environmental concern because of the waste generated. On the other hand, microbial contamination of food is a serious problem affecting the human health and the food industry. Accordingly, any attempt to use biocompatible or biodegradable packaging materials and, eventually, exhibiting bactericidal capacity, becomes indispensable. Cellulose and chitosan are, biocompatible and biodegradable polymers with a quite similar molecular structure that makes possible the formation of homogeneous blends [1].

Many studies have been conducted looking to increase the chitosan applicability as bactericidal agent. These studies include its mixture with other biopolymers, synthetic polymers, and inclusion of nanoparticles as active agents [1][2][3]. In this regard, Zinc oxide (ZnO) has been recognized by the Food and Drug Administration (FDA) as safe material GRAS (21 CFR 182.8991), and its apparent bactericidal character has aroused great interest; however, ZnO application would depend on how well the powdered material is fixed within a safe matrix. To control and enhance the ZnO properties, this can be doped with Li, Al, Mn among other elements. Zn^{+2} and Mg^{+2} ionic radius are 0.74Å and 0.65Å respectively, which suggest the capability to form solid solutions of the type $Zn_{1-x}Mg_xO$. Moreover, it has been suggested that doping with Mg improves the bactericidal capacity [4].

An alternative to face these concerns is the use of biopolymers-based nanocomposites, which are biodegradable and can be modified to provide protection against bacteria based on the tunability of their functional properties. On this basis, the present work

focuses on the fabrication of chitosan/cellulose films hosting ZnO nanoparticles as an attempt to produce nanocomposites with bactericidal capacity.

1.1 Motivation

Currently, the large majority of packaging used in the food industry are made from synthetic materials derived from fossil fuels, which are not biodegradable and increase the environmental contamination [5][6]. This situation promotes the search for environmental friendly materials that can maintain the food quality and extend its shelf life. In this sense, the biopolymers are an alternative for food packaging, as compared to synthetic materials, these come from renewable natural resources, are abundant, inexpensive and biodegradable [5]. Researches with chitin, chitosan, alginate, starch, show the possibility of using these materials in the food and packaging industry [1][5][7][8] [9][10].

Chitosan is a linear polysaccharide obtained from the n-deacetylation of chitin, possesses gel and film forming properties, a large metal complexation capacity and antimicrobial characteristics, which has received much attention [5][6][7][11]. Has been reported that the bactericidal character of chitosan is due to the amino group is able to interact with the cell membrane of microorganisms, causing a leakage of intracellular material [6].

Meanwhile, the cellulose is the most abundant biopolymer in the earth, this polysaccharide consists of a linear chain of β (1 → 4) linked D-glucose units, tends to form crystals using the intermolecular hydrogen bonds. Can be used as emulsifier, stabilizer, dispersant and as filler to improve the mechanical and barrier properties of the

composites [12]. Therefore it is expected that the addition of cellulose improves the mechanical properties of chitosan.

Microbiological contamination is another problem facing the food industry, this can cause diseases that attempt against public health. The abuse of drugs and antibiotics has contributed to the development of resistant strain bacteria, so it has become necessary to find new strategies to control the growth of microorganisms [8][13]. Nanotechnology can provide solutions to the challenges of the food industry and has developed nano-structured materials that can be used as antibacterial agents. Nanoparticles of silver, gold, copper, zinc, zinc oxide, titanium oxide, among others, have been synthesized and have shown their biocidal effect against various types of microorganisms [8][13][14][15].

The bactericidal character of zinc oxide has aroused great interest, and has been included in the list of substances generally recognized as safe (GRAS) generated by the Food and Drug Administration in the United States (21 CFR 182.8991). This semiconductor material has high thermal and chemical stability a band gap of 3.3 eV and a binding energy of 60 meV, is environmentally friendly and can absorb ultraviolet light. These properties make zinc oxide having multiple applications such as photovoltaic solar cells, electrical devices, optical coatings, antibacterial coatings, among others [16][17].

The zinc oxide nanoparticles exhibit better bactericidal capacity than the bulk ZnO due to its small size (less than 100 nm), this allows better interaction with the bacteria. Hydrothermal synthesis, sol-gel, alkali precipitation, emulsion precipitation, are common methods used to synthesize them [16]. It is still unclear what the mechanism of bactericidal action of ZnO nanoparticles. However, studies suggest that zinc oxide when

is activated by Ultra Violet light generated hydroxyl radicals, superoxide and hydrogen peroxide, reactive oxygen species that can damage the bacterial cell [8][18].

The Zinc Oxide at nanoscale is a suitable candidate for its possible application in food packaging systems due his bactericidal properties, which can be improved by doping process with Mn, Co, Mg, Sn, Li, Al among other elements [4][19]. Zn^{+2} and Mg^{+2} have very similar ionic radii, which suggest the capability to form solid solutions of the type $Zn_{1-x}Mg_xO$. Moreover, the literature reported that Mg-doping improves the bactericidal and UV blocking capacity [4].

Various studies report that the incorporation of active compounds in packaging materials is a viable alternative to inhibit the growth of microorganisms and maintain the quality and food safety. In this research the effect of adding cellulose on the mechanical properties of films chitosan will studied, also the synthesis and incorporation of zinc oxide nanoparticles in chitosan-cellulose matrix to obtain a composite with improved bactericidal properties. The bactericidal properties of ZnO nanoparticles and nanocomposites will be evaluated against *E. coli* because is a foodborne microorganisms potentially hazardous in food industry.

1.2 Objectives

1.2.1 Main

- Assess the bactericide effect of pure and Mg-Doped ZnO nanoparticles, naked and dispersed within a biopolymer matrix, for potential applications in the food industry.

1.2.2 Specifics

- Determine optimum conditions to synthesize ZnO nanoparticles in polyol media.
- Characterize ZnO nanoparticles from a structural, morphological and functional viewpoints.
- Asses the bactericidal properties of pure and Mg doped zinc oxide nanoparticles
- Determine optimum synthesis conditions of chitosan and chitosan/cellulose bare films.
- Determine structural and mechanical properties of chitosan/cellulose blend films as a function of cellulose content.
- Determine mechanical properties of chitosan/cellulose/ZnO nanocomposites as function of nanoparticles loading and composition.
- Evaluate the bactericidal properties of Chitosan/Cellulose/ZnO nanocomposites as function of nanoparticles loading and composition.

1.3 Thesis contents

In the first chapter of this thesis the motivation and objectives of the research work will be presented. Chapter II theoretical background includes the review of the main concepts involved with the research, as well as the description of the action mechanism antibacterial of Zinc Oxide nanoparticles and Chitosan.

In chapter III, the experimental methods to synthesize pure and Mg doped ZnO Nanoparticles and fabricate chitosan/cellulose blend films and chitosan Celulose ZnO-Mg nanocomposite including structural, morphological, optical characterization and mechanical properties will be present. As well as the assays bactericidal against *Escherichia coli* and the water vapor permeability for blend films and nanocomposites. Both chapters IV and V were focused on the discussion and interpretation of the results.

CHAPTER II: THEORETICAL BACKGROUND

2.1 Nanotechnology in the food Industry.

Nanotechnology has many potential applications in various branches of the food industry, (Figure 1) mainly in processing, quality control, packaging and safety. Research in these areas are related to packaging and food products with additives at nanoscale, which could be used as encapsulates of smell and taste, gas or pathogens sensors, temperature abuse sensors, bactericidal agents, among others [20].

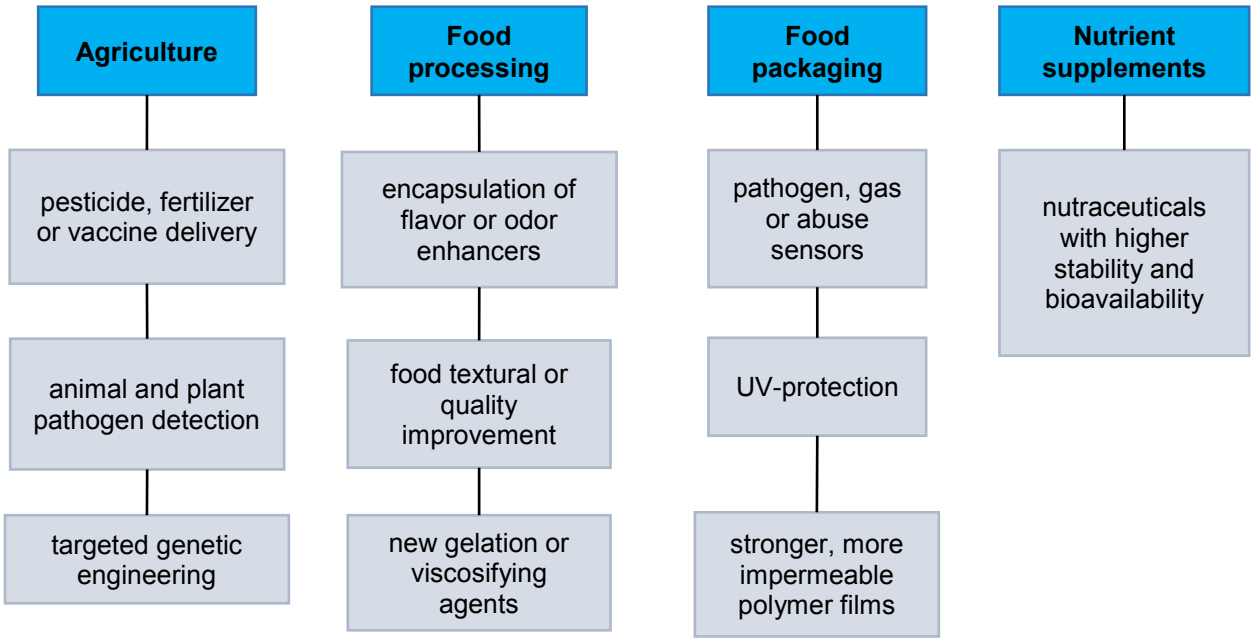

Figure 1 Diagram of potential applications of nanotechnology in food science [20]

The packaging area is the most developed and investigated because of the need to find better materials to protect food from moisture, oxygen, light, microorganisms and other factors of deterioration. Several studies have focused on the synthesis of impermeable packaging, nano sensors, nano-covered with bactericidal properties and polymeric

nanocomposites that increase the safety and shelf life of the food product thus preserving its flavor, color, texture, and other properties [20][21].

Some studies have evaluated the use of antimicrobial nanoparticles (such as silver nanoparticles, zinc oxide, magnesium oxide, etc.) to extend the shelf life of products and reduce the growth of microorganisms, this nanoparticles can be incorporate into polymeric matrix forming nanocomposites of great interest, and that increase the mechanical strength, thermal stability and improve the barrier properties of packaging materials [21].

Cellulose, chitin, chitosan, starch, alginate, polylactic acid, are some of the polymers which have been investigated as potential bio-matrices to produce nanocomposites usable in the food industry.

2.2 The disperse nano-phase: Zinc Oxide based nanoparticles.

Zinc oxide is a II-VI semiconductor, abundant in nature, with high thermal and chemical stability, a band gap of 3.3 eV and an exciton binding energy of 60 meV. Because of its optical, electrical and thermal properties, ZnO has very diverse applications such as solar cells, optical coatings, electrical and optical devices, among others [17][22]. Currently, nanoscale ZnO has received much attention; ZnO bactericidal properties and biodegradability have expanded its potential uses to other areas such as biomedicine, food industry, and pharmaceutical industry. In addition, ZnO non-toxicity makes it a suitable material for biological applications.

2.2.1. Structural properties

Zinc oxide can exist in 3 crystalline structures: hexagonal wurtzite, cubic zinc blend and cubic rock salt. The ZnO wurtzite phase is the most thermodynamically stable at ambient conditions, the zinc blende is metastable and can be stabilized only by epitaxial growth on cubic substrates, and the rock salt (NaCl type) can be obtained and stabilized only at high pressures. Figure 2 shows the crystal structures of ZnO [22].

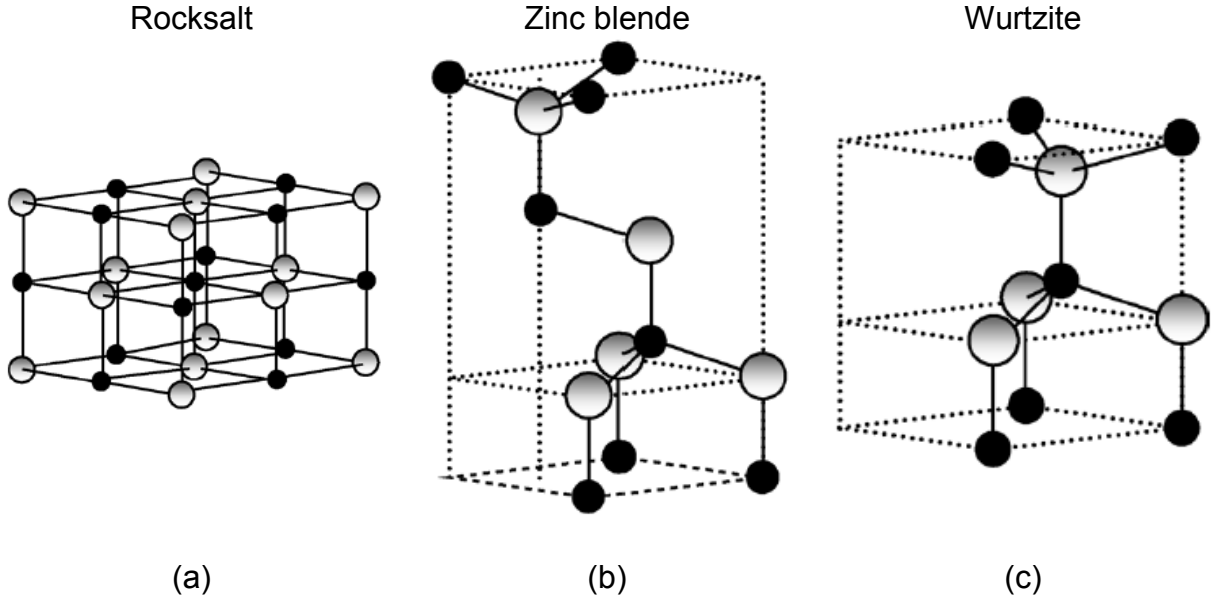

Figure 2 Stick-and-ball representation of ZnO crystal structures: (a) cubic rocksalt, (b) cubic zinc blende, and (c) hexagonal wurtzite.
Shaded gray and black spheres denote Zn and O atoms, respectively [23].

ZnO wurtzite phase is the most stable, since the electronegativity difference between zinc and oxygen causes repulsion between them. In this structure (Figure 3), each zinc atom (Zn^{2+}) is surrounded by a tetrahedron of four oxygen atoms (O^{2-}) and vice versa, and has

a hexagonal cell with Two lattice parameters "a" and "c" whose values under normal pressure and temperature are 3.253Å and 5.213Å respectively [24].

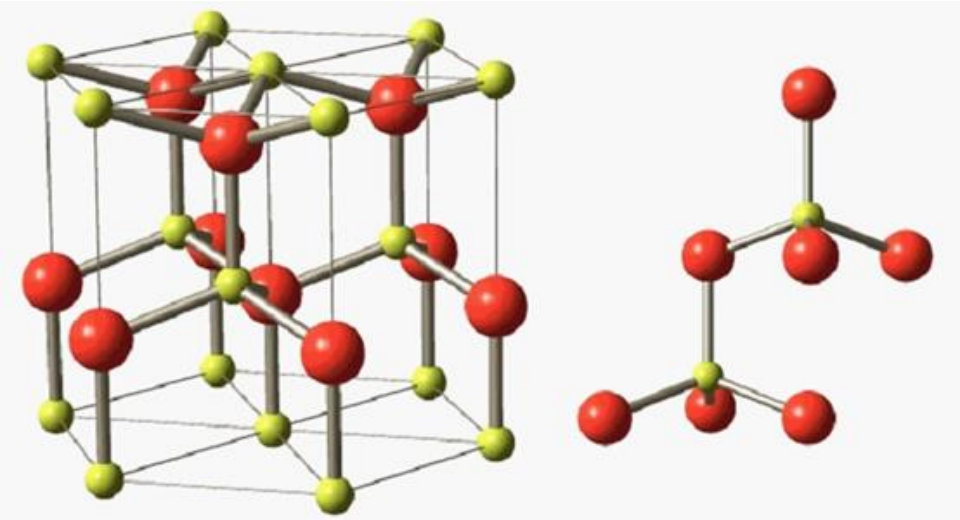

Figure 3 ZnO crystalline structure-Wurtzite yellow and red spheres denote Zn and O atoms, respectively [25].

2.2.2 Bactericidal Properties and Mechanism of ZnO

The food industry has incorporated zinc oxide in cans of fish, meat and grains to preserve color and to prevent the deterioration of these; ZnO has also been used as a source of Zinc in fortified foods. Recently, ZnO nanoparticles have aroused great interest because of their very promising bactericidal capacity, which is higher when compared with the bulk ZnO [18]. Several studies have reported that ZnO nanoparticles have an antibacterial effect against *Escherichia coli*, *Salmonella*, *Listeria monocytogenes*, *Staphylococcus aureus*, *Campylobacter jejuni*, among other microorganisms; however, the mechanism of antibacterial action is still unclear. It has been proposed that ZnO can be activated by UV and visible light and generate in the presence of moisture, Reactive Oxygen Species

(ROS) such as hydroxyl radicals (OH^-), superoxides and hydrogen peroxide (H_2O_2) [13][18].

It has also been suggested that the hydroxyl radicals and superoxide due to its negative charge cannot penetrate the cell membrane, so they remain in contact with the outer surface of the bacteria causing damage to proteins, lipids and DNA; in contrast, hydrogen peroxide can penetrate the membrane and damage bacterial cells.

Reactive oxygen species are very small and highly reactive molecules, because have a layer of valence electrons unpaired; their generation is carried out from molecular oxygen, which is partially reduced to produce superoxide ($^{\bullet}O^-_2$) and this in turn produces hydrogen peroxide (H_2O_2). When hydrogen peroxide is reduced partially it produces the hydroxyl radical (OH^-), the most reactive of the oxygen species, which can oxidize any cellular macromolecule to which it attaches [26]. Meanwhile, singlet oxygen is the energetically excited forms of molecular oxygen, their main method of production requires the presence of a photosensitizer (PS), which is activated at a specific wavelength generated by an external source.

The reactive oxygen species (ROS) including singlet oxygen may affect the metabolic processes, moreover produce an oxidative stress, which may injure bacterial cells by oxidation of membranes, enzymes, proteins, DNA, and polyunsaturated fatty acids in lipids [26].

The zinc oxide nanoparticles exhibit better bactericidal capacity than the bulk ZnO due to its small size (less than 100 nm) and high surface area, this allows better interaction with the bacteria [27]. Some studies have evaluated the effectiveness of zinc oxide

nanoparticles to kill bacteria comparing different particle sizes, and has been found that the smaller particles show a greater inhibition of bacterial growth than large particles (> 1 mm). It has also been reported that ZnO nanoparticles (7nm) produce a greater cellular internalization and bacterial cell damage when compared with larger particles (260 nm and 800) [28].

MgO is a non-toxic and biocompatible material, has high thermal stability, low cost and has been suggested as an antibacterial agent [29]. Zn^{+2} and Mg^{+2} have very similar ionic radii, which suggest the capability to form solid solutions of the type $Zn_{1-x}Mg_xO$. Moreover, the literature reported that Mg-doping improves the bactericidal and UV blocking capacity [4]. For the above, it would be expected that the synthesis of a nanostructure containing Zn and Mg species have a synergistic effect and therefore an increase occurs in the antimicrobial activity.

2.3 The matrix: Chitosan/Cellulose

2.3.1 Chitosan

2.3.1.1 Origin

The chitin is the second most abundant natural polymer that is present, as crystalline microfibers in the exoskeleton of insects and crustaceans, and cell wall of fungi and yeasts. It was discovered in fungi by Henri Braconnot in 1811, it was initially called "fungine". In 1823 he was isolated from the wings of a beetle and received on behalf of "chitin" [30][31][32]. The Figure 4 show the origin of chitin from crustacean; crustacean waste generated by fishing and food industries are used for the production of chitin. These

wastes are subjected to deproteinization with NaOH, followed by a demineralization generally using HCl, and discoloration with $KMnO_4$ [33][34].

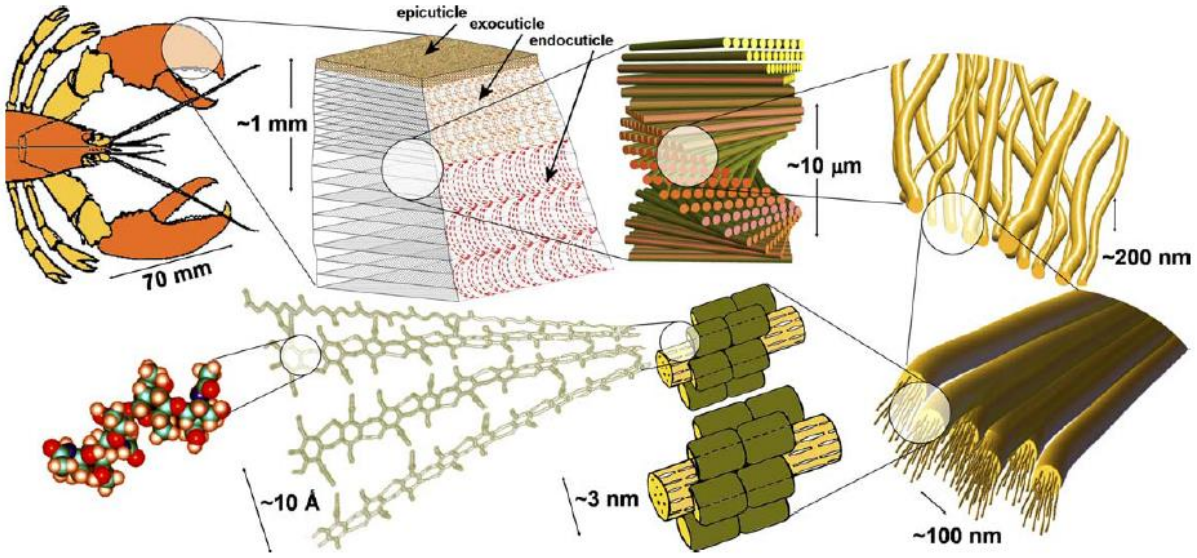

Figure 4 Origin of chitin from crustacean [35]

Chitosan is a derivative of chitin, was discovered in 1859 by Rought. It can be obtained by enzymatic hydrolysis using chitin deacetylasa. Industrially it is obtained by a process of deacetylation and depolymerization, in which solutions of NaOH (40-50%) at temperatures above 60 ° C are used to remove the acetyl groups present in the chitin and reduce its molecular weight. The molecular weight and degree of deacetylation depending on the conditions to which the reaction occurs, for chitosan these values range from 10.000 to 1,000,000 Daltons and 50-95% respectively, while for the chitin are among 1 to 2.5 million Daltons and the deacetylation degree is less than 10% [30][31][32][36].

2.3.1.2 Chemical structure

Chitosan and Chitin are linear polysaccharides formed by monomeric chains of glucopyranos (N-acetylglucosamine and glucosamine) linked by β- (1-4) bonds. The chemical structure of these polymers differs in that the acetamide group at position C2 of chitin is replaced by the amine group in chitosan [36].

In Figure 5, chemical structure of both biopolymers is shown. It is considered chitin if the acetyl group is present in more than 50% of the carbon rings and is chitosan if less than 50% have the acetyl group.

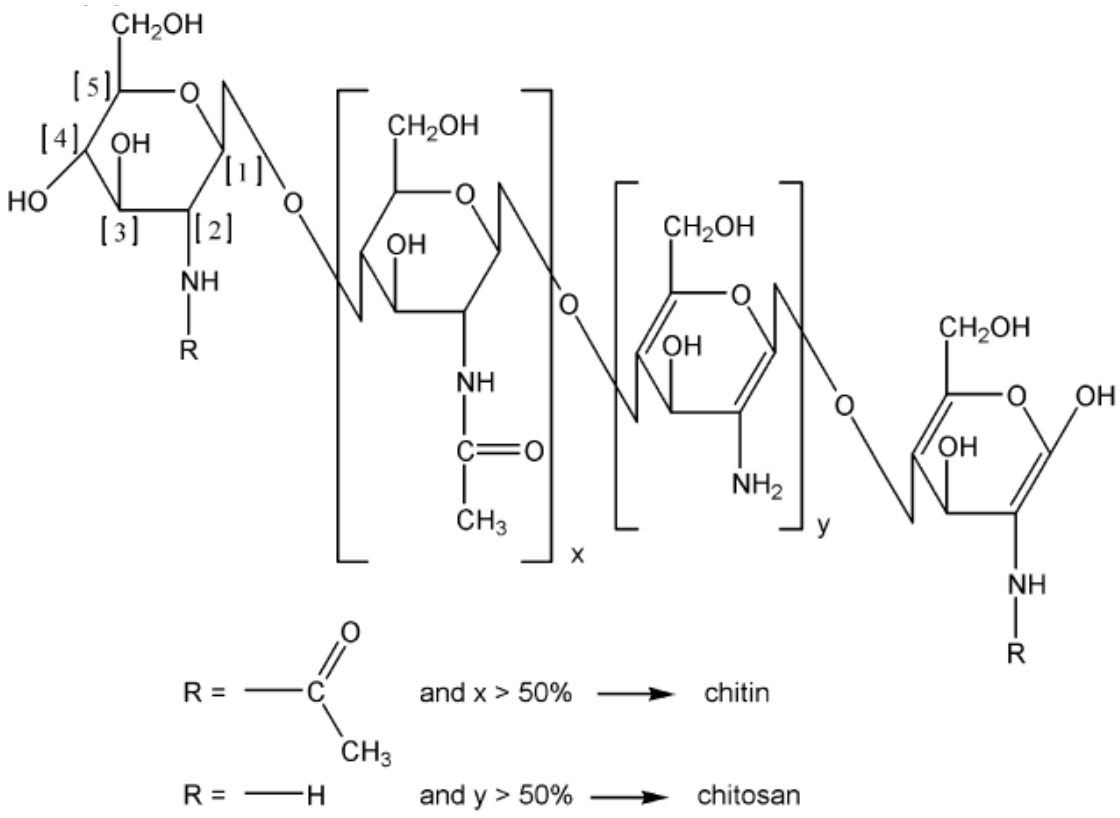

Figure 5 Chemical structure of chitin and chitosan [31]

The presence of hydroxyl, amino and acetamide groups in the structure of chitosan gives it a variety of chemical and biological properties that can be modified to extend their applications; these reactive groups are suitable for cross-linking and chemical activation. Among the properties of chitosan can be noted that it is highly hydrophilic, crystalline and soluble in dilute aqueous acidic solutions, has chelating, complexing, flocculant, antibacterial and film forming properties [36].

2.3.1.3 Applications

Chitosan is a biocompatible, biodegradable, non-toxic material having antimicrobial properties and can be easily transformed into gels, films, fibers, beads and nanoparticles; so it has been studied in various fields such as medicine and pharmaceuticals, agriculture, food industry, in water treatment, among others.

In agriculture it is used as biological control, to provide protection to the plant against pests and diseases, one of the techniques used is the controlled release of biocides or antimicrobial agents fixed in a matrix of chitosan. Also it reported antifungal activity of chitosan against *Aspergillus niger*, *Alternaria alternata* and *Rhizopus oryzae*, which is attributed to its polycationic nature that can cause changes and alterations in the cells of fungi [37].

In the medicine and pharmacy field has been evaluated using chitosan beads as matrix in drug delivery systems, also sponges, bandages and gels have been synthesized for the treatment of wounds, ulcers and burns; because it has been found that chitosan helps promote healing and tissue growth [38].

Due to its non-toxicity, low cost and high efficiency (related to amino and hydroxil groups that function as binding sites) chitosan has been used in wastewater treatment as a coagulant to reduce turbidity and alkalinity; and as a flocculant to remove solid colloidal particles. Also has been reported its use in the recovery of heavy metals, pesticides, phenols and dyes, this adsorption capacity is related to its crystallinity, surface area, porosity and particle size [39].

2.3.1.4 Bactericide capacity of chitosan

Chitosan has shown bactericidal activity (kills bacteria) and bacteriostatic (inhibits growth of bacteria) against pathogens and spoilage microorganisms. Several mechanisms have been proposed to explain the antimicrobial properties of chitosan, which have been attributed to the reactive groups (amino group and hydroxyl groups) present in its structure. The first and most accepted, provides that the amino group positively charged of chitosan interacts with the negatively charged of bacterial membrane affecting its permeability and generating leakage of intracellular material. The second explains that chitosan can penetrate the cell and interact with its DNA to inhibiting the protein and mRNA synthesis. The third says that the chitosan acts as a chelating agent, linking essential nutrients, metals and enzymes necessary for bacterial growth. The fourth proposed that the chitosan avoids the entrance of nutrients into the cell, forming a polymeric membrane around [34][40].

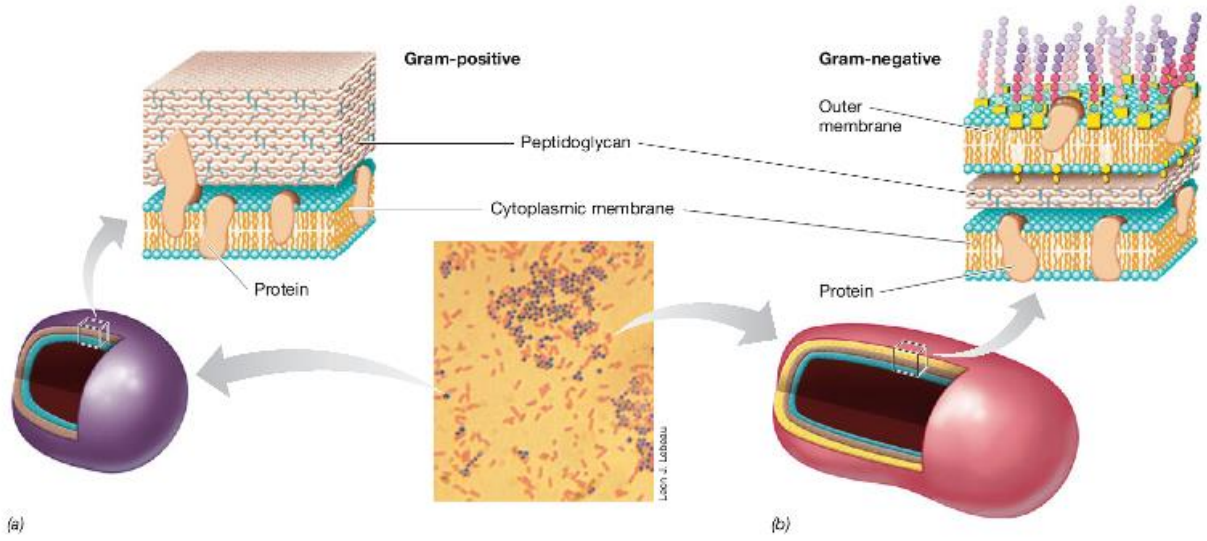

Figure 6 Cell walls of Gram positive (a) and negative gram (b) bacteria [41]*. The photo in the center shows cells of* Staphylococcus aureus *(purple, gram-positive) and* Escherichia coli *(pink, gram-negative)*

The bactericidal activity of chitosan depends on several factors, among which can be highlighted the type of bacteria, the pH and solution concentration, molecular weight, degree of polymerization and deacetylation of chitosan chains. The bacteria can be Gram negative or Gram positive (Figure 6). In the case of Gram negative bacteria, which are surrounded by an outer membrane and possess a thin but complex cell wall (formed by proteins, lipids, polysaccharides and peptidoglycan), it has been proposed that low molecular weight (LMW) chitosan, can enter the cell and cause its deterioration or bind to DNA and inhibit reproduction. In contrast in the case of the cell wall of Gram positive bacteria, which is much thicker and consists of peptidoglycan and protein, the chitosan inhibits the entry of nutrients forming a polymer membrane on the surface of the cell. If the chitosan has a high molecular weight (HMW), it will be linked to the outer membrane of the bacterium affecting permeability and nutrient transport [34][40].

It has been found that the bactericidal activity of chitosan increases with decreasing pH below 6.3, because the ionization of the amino group that is conducive to a better interaction with the negative surface charge on the bacteria. Likewise, the bactericidal capacity increases with the degree of deacetylation in the chitosan; the higher deacetylation will promote a large presence of amino groups, with the subsequent enhancement of the positive charge on bacterium surface. Moreover, a high concentration of dissolved chitosan species would also provide a strong positive surface charge on the surface of the cell, keeping it in suspension and preventing the transport and exchange of materials with the surrounding medium; in turn, low concentrations of dissolved chitosan species would favor agglutination by binding to negatively charged membrane, this destroys the membrane and facilitates the leakage of nutrients [40].

2.3.2 Cellulose

2.3.2.1 Origin

Cellulose is the most abundant renewable polymer on earth and was discovered in plants by Anselme Payen in 1838. It is a structural material, organized as microfibers bonded together, and is part of the supporting tissues of plants, can also be bio-synthesized by some bacteria as *Acetobacter xylinum*. The Figure 7 shows the origin of cellulose from plants. The cellulose derived from plants is more used due to its low production cost, but must be separated from other substances such as hemicellulose, lignin, pectin and wax, while the bacterial cellulose is more pure and can be produced with a molecular weight

and degree of polymerization known if the fermentation process conditions are controlled [42] [43].

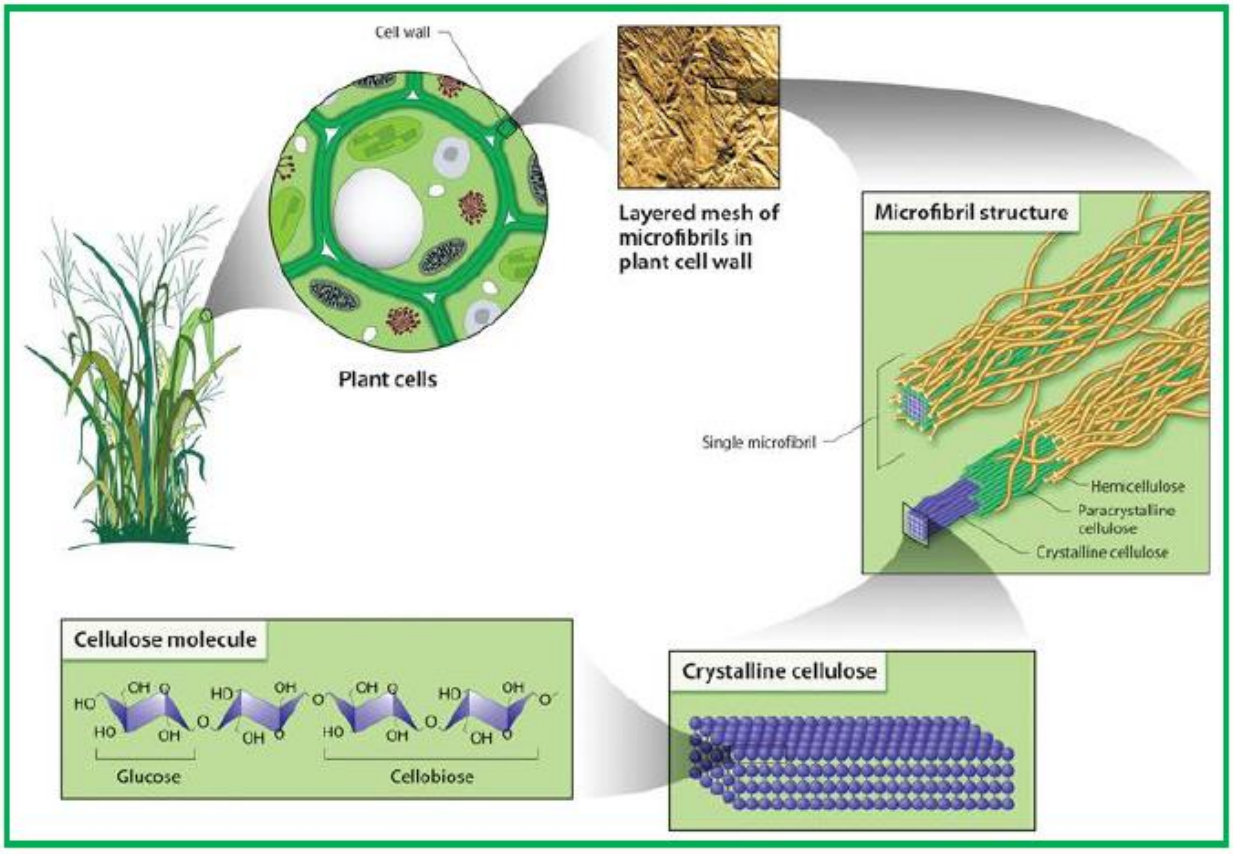

Figure 7 Origin of cellulose from plants [43]

2.3.2.2 Chemical structure

Cellulose is a homopolysaccharide, with the common formula $(C_6H_{10}O_5)n$, consists of a linear chain composed of units β-D glucopyranose linked by β- (1-4) bonds. Cellulose chains in nature have a degree of polymerization of approximately 10000, while for the cellulose from cotton this value is about 15000 [42][43].

Figure 8 shows the chemical structure of cellulose. The presence of hydroxyl groups plays a fundamental role in its crystalline arrangement and allows the formation of multiple hydrogen bonds intra- and inter molecular making it insoluble in water and most common solvents. However, these hydroxyl groups can be modified chemically to obtain derivatives with greater solubility, also to improve their properties and expand their applications [43][44].

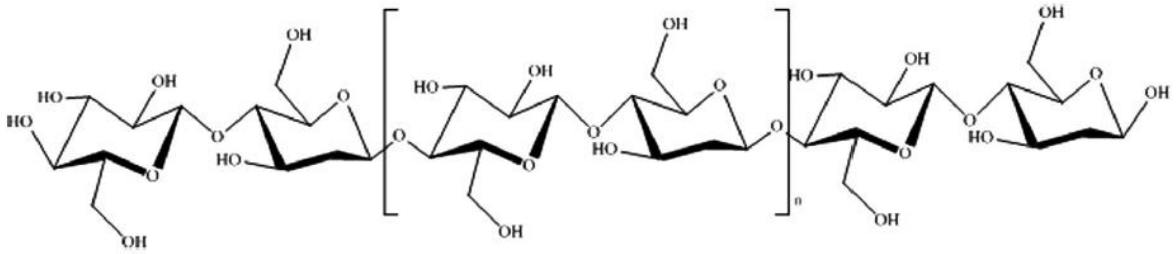

Figure 8 Chemical structure of Cellulose [42]

2.3.2.3 Applications

Cellulose is a biodegradable, hydrophilic material, which has no smell, no taste [44], normally used in the production of paper, paperboard, textiles, construction materials and explosives. Diverse forms of cellulose (as crystallites, nanocrystals, whiskers, nanofibrils, and nanofibers) have aroused great interest in other areas such as biomedicine, the water treatment and the food packaging industry because of its properties and low cost [45].

The literature reports that cellulose can be chemically modified because of the hydroxyl groups present in its structure to improve its adsorption capacity. In this way, cellulose based adsorbents materials which are used in the removal of heavy metals and other contaminants present in water are obtained [45].

Cellulose has high-strength, high stiffness and low density, for this reason is also used to increase the mechanical properties and biodegradability of polymeric composites, in this sense is incorporated as a filler to reinforce plastics. It has reported the use of cellulose from pineapple leaf to reinforce a polymeric matrix polyurethane for the purpose of study their potential applications in the biomedical field [46].

Similarly has been investigated use of cellulose fibers to reinforce hydroxypropyl methylcellulose films in order to improve its mechanical and barrier properties for use as packing material in the food industry [47].

High Density Polyethylene (HDPE), polypropylene (PP), Low Density Polyethylene (LDPE) and Polyethylene Terephthalate (PET) are packing materials more currently used, each of these has unique properties that determine their application. Table 1 shows the mechanical properties and the Water Vapor Transmission Rate for each one of these.

Table 1 Mechanical and barrier properties of Common Food Plastics [48][49]

Material Characteristic	**HDPE**	**LDPE**	**PP**	**PET**
Density (g/cm^3)	0.959	0.925	0.905	1.35
Tensile Strength (MPa)	22.1 - 31.0	8.3-31.4	31.0-41.4	48.3-72.4
Percent Elongation (%)	10-1200	100-650	100-600	30-300
Water Vapor transmission (nmol/m^{2}s)	3 - 6.5	12	5 - 6.5	13

Most materials used in food packaging are not biodegradable and remain in the environment for hundreds of years, polluting the oceans and the land, have also generated a global waste disposal problems. Currently, the use of biopolymers (such as starch, cellulose, chitosan, alginate among others) is being explored to develop eco-friendly food packaging materials. The biopolymers are biodegradable, abundant in

nature and have good film forming properties. Addition to this, mechanical and barrier properties can enhanced by adding reinforcements or fillers at nanoscale, which could also improve its antimicrobial properties [50][51].

2.4 *Escherichia coli* [52]

Escherichia coli was isolated from childrens' faeces by Theodor Escherich in 1885, initially was called Bacterium coli. This microorganism lives in the intestines of humans and warm blooded animals where is the predominant facultative anaerobe and part of the essential intestinal flora. An image of *Escherichia coli* is shown in the Figure 9.

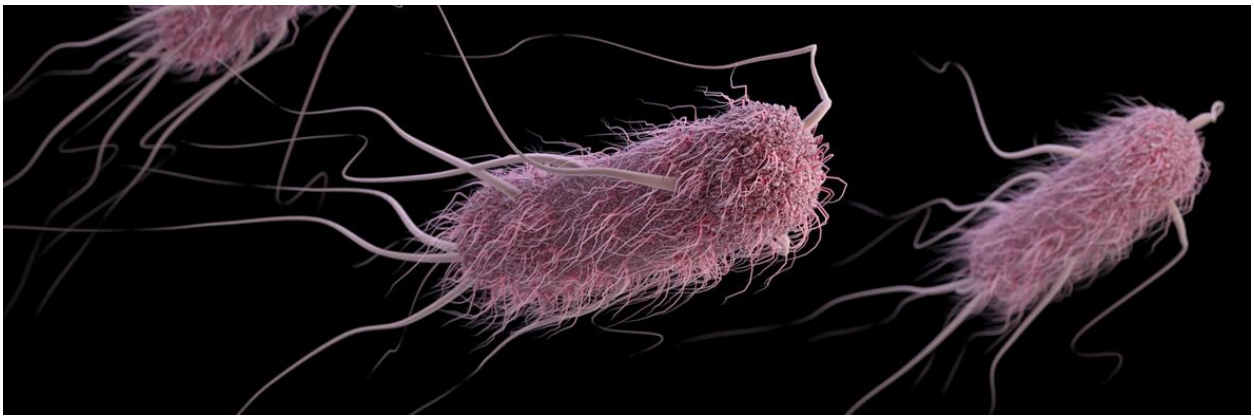

Figure 9 Escherichia coli [53]

E coli is a Gram-negative bacillus, member of the *Enterobacteriaceae* family, (which includes pathogens such as *salmonella*, *Shigella* and *Yersinia*), is a typical mesophile growing from 7-10°C up 50°C with optimal growth temperature around 37°C. It is catalase-positive, oxidase negative, and no spore-forming, and can be mobile by the presence of flagella.

Due to its abundance in human and animal feces and their ability to survive in water, the presence of *E. coli* in water or food, is now regarded as an indicator of recent fecal contamination and the possible presence of enteric pathogens.

The most strains of *E. coli* are harmless, however they can be an opportunistic pathogen and cause infections in immunocompromised hosts. Also, have emerged a group of pathogenic strains that cause diarrheal illness in humans, which are classified as *enterotoxigenic E. coli (ETEC), enteropathogenic E. coli (EPEC), enteroinvasive E. coli (EIEC), enterohemorrhagic E. coli (EHEC), diffusely adherent E. coli (DAEC)* and *Enteroaggregative E. coli (EAEC)*, of these only the first 4 groups have been implicated in foodborne illness.

In this work the bactericidal capacity of zinc oxide nanoparticles and nanocomposites synthesized has been evaluated against Escherichia coli (ATCC® 35218 ™). Studies have reported that E. coli ATCC® 35218™ is a suitable surrogate because it allows to model the behavior of a BSL 2 type pathogen like E. coli O157: H7 [54].

2.5 Literature review

Some studies related to zinc oxide and the study of their properties reported in the literature are registered in Table 2. The synthesis method, the precursor and the surfactant agent varies from one to another. In turn, some studies related to blend films and polymeric nanocomposites are registered in Table 3.

Table 2 Previous works on ZnO nanoparticles

Title	Research details	Main Results	Main Concerns
Antibacterial Activity and Mechanism of Action of Zinc Oxide Nanoparticles against *Campylobacter jejuni* [27]	Investigated the mechanism of action of ZnO nanoparticles against *C. jejuni* by examining cell morphology, membrane permeability, and gene expression through the utilization of scanning electron microscopy and advanced molecular.	• Inactivation of *Campylobacter jejuni* was obtained with 0.03 mg/ml of ZnO nanoparticles (commercially acquired with an average particle size of 30 nm)	• The nanoparticles were not synthesized.
Preparation and characterization of ZnO nanoparticles by a novel sol–gel route [55]	ZnO nanoparticles were prepared by sol-gel route using TEA (triethanolamine) as a surfactant and zinc acetate dihydrate (ZnAc) as precursor. The best concentration of each component was adjusted comparing the different absorption spectra.	• Sols containing ZnO nanoparticles with 3 to 4 nm size and spherical shape. • The peak characteristic in absorption spectrum was around 275 nm.	• Sols with a low percentage of ZnO and a huge amount of organic complexes. • The nanoparticles were not recovered from the sol.
Influence of Mg doping level on morphology, optical, electrical properties and antibacterial activity of ZnO nanostructures [4]	Mg doped ZnO nanostructures with varying Mg doping levels (i.e. 0, 3, 5 and 10 at. %) were synthesized by co-precipitation technique using distilled water as a solvent and ZnCl2, MgSO4-7H2O as precursor. The antibacterial activity was evaluated by culture turbidity and zone of inhibition methods towards *S. aureus* and *Pseudomonas aeruginosa*.	• The average crystallite sizes were 26 nm for undoped ZnO to 22 nm for 10% Mg doped ZnO. • The peak characteristic in absorption spectrum was around 364 nm. • The band gap energies are found to be 3.40, 3.47 and 3.49 eV for undoped ZnO, 5% and 10% Mg doped ZnO samples, respectively • Antibacterial activity towards *S. aureus* and *P. aeruginosa*, the synthesized nanostructures have inhibited almost 90% growth rate of both bacterial strains	• Nanoparticles aggregation

Table 3 Previous works on polymeric films and nanocomposites

Title	Research details	Main Results	Main Concerns
Biocomposite films prepared from ionic liquid solutions of chitosan and cellulose [3]	Preparation of chitosan/cellulose porous films with chitosan contents ranging from 5 to 50 wt% using 1-butyl-3-methylimidazolium acetate (BMIMAc) as solvent media.	• Formation of homogeneous chitosan and cellulose blends • The thickness of the films varied between 1 mm and 1.2 mm. • The morphology of the polymeric blends depends on the chitosan–cellulose weight percent ratio.	• Use of sophisticated equipment • No systematic synthesis
Study on microstructure and physical properties of composite films based on chitosan and methylcellulose [56]	Biodegradable films were obtained from chitosan (CH) and methylcellulose (MC) solutions. These solutions were mixed with the CH: MC (w/w) proportions: 25:75, 50:50 and 75:25 and dried at 60 °C in a ventilated oven to constant weight.	• Homogeneous, thin, flexible and transparent films were obtained • Thickness of films varied between 14.12 ± 1.59 and 26.07 ± 3.17 μm, • Percent elongation values of films were 12.7% for MC, and 3.9% for CH and intermediate values were obtained with composite films	• methylcellulose (MC) increased film solubility
Preparation, characterization and antibacterial applications of ZnO-nanoparticles coated polyethylene films for food packaging [13]	In situ preparation of ZnO nanoparticles onto starch-coated polyethylene film, using a aqueous solution of zinc sulphate, then a aqueous solution of sodium hydroxide and heat treatment at 70 ◦C for complete conversion of $Zn(OH)_2$ into ZnO. The biocidal action against *Escherichia coli* of ZnO loaded film was tested using zone inhibition and killing kinetics of bacterial growth methods.	• The excitation absorption peak of ZnO particles is observed at nearly 364 nm • a clear zone of inhibition around the ZnO-loaded SCP film was observed, whereas a dense population is observed in the Petri-plate containing plain film	• Use of synthetic polymers. • Samples with impurities derived from the synthesis of the nanoparticles

Table 3 Previous works on polymeric films and nanocomposites (continuation)

Title	Research details	Main Results	Main Concerns
Zinc oxide nanoparticles loaded active packaging, a challenge study against Salmonella typhimurium and Staphylococcus aureus in ready-to-eat poultry meat [8]	Zinc oxide nanoparticles were prepared by hydrothermal synthesis using zinc chloride in aqueous solutions of sodium hydroxide. ZnO nanoparticles were loaded on film of calcium alginate for prepare an active packaging. The antibacterial activity of the nanoparticles and films was determined against *Salmonella typhimurium* and *S. aureus* in solid and liquid media using nutrient agar and broth and Zone of inhibition method.	• Spherical nanoparticles with average size about 50 nm • Zinc oxide nanoparticles concentrations ≥0.1 mg/mL were found lethal for both of the target bacteria • The tensile strength (TS) decreased with the addition of ZnO, for control film were 4.75 ± 0.51 N/cm2, whereas for 1 and 3 mg/mL ZnO nanoparticles loaded film were 3.35 ± 0.06 and 2.35 ± 0.29 N/cm2 respectively. • The ZnO nanoparticles loaded films showed the clear inhibition zone against the target bacteria.	• Agglomerates of nanoparticles on the polymer matrix. • Low tensile strength

CHAPTER III: EXPERIMENTAL

3.1 Materials selection

All regents were of analytical grade and used without any further purification. Chitosan (Medium molecular weight, Sigma Aldrich), Cellulose (Microcrystaline powder, Sigma Aldrich), 4-Methylmorpholine-N-oxide (NMMO Solution 50% wt. in H2O, Sigma Aldrich) and Acetic Acid (99.7%, Alfa Aesar) were used for the polymeric and nanocomposite films fabrication.

Zinc acetate dihydrate ($Zn(CH_3COO)_2 \cdot 2H_2O$, ACS, 99%, ACROS Organics), Magnesium acetate tetrahydrate ($Mg(CH_3COO)_2 \cdot 4H_2O$, ACS, 98%, Alfa Aesar) and Triethylene Glycol (TEG, 99%, Alfa Aesar) were used for the synthesis of the pure and Mg-doped Zinc Oxide Nanoparticles.

3.2 Materials synthesis

3.2.1 Synthesis of pure and magnesium doped ZnO nanoparticles

The synthesis of pure ZnO nanoparticles was conducted via modified polyol method using Zinc acetate in TEG at a concentration of 0.08 mol / L. The reaction temperature was maintained at 180 ± 2 °C under reflux and vigorous stirring conditions for 30 minutes. The resulting suspension was quenched in a cool bath at 4ºC to stop the reaction and avoid crystal growth under slow cooling conditions. Then, the nanoparticles were recovered by centrifugation at 8,000 rpm for 30 minutes and washed using ethanol and ethyl acetate. This washing cycles were repeated for three times. The nanoparticles were dried at room conditions [57][58].

For the synthesis of magnesium doped ZnO nanoparticles, Zinc acetate and Magnesium acetate were mixed in TEG according to $Zn_{1-x}Mg_xO$ stoichiometry following the procedure described on Figure 10. The dopant concentration was in the range of 0 to 10 at. % [59]. Figure 11 show the experimental set up used in the synthesis of the nanoparticles.

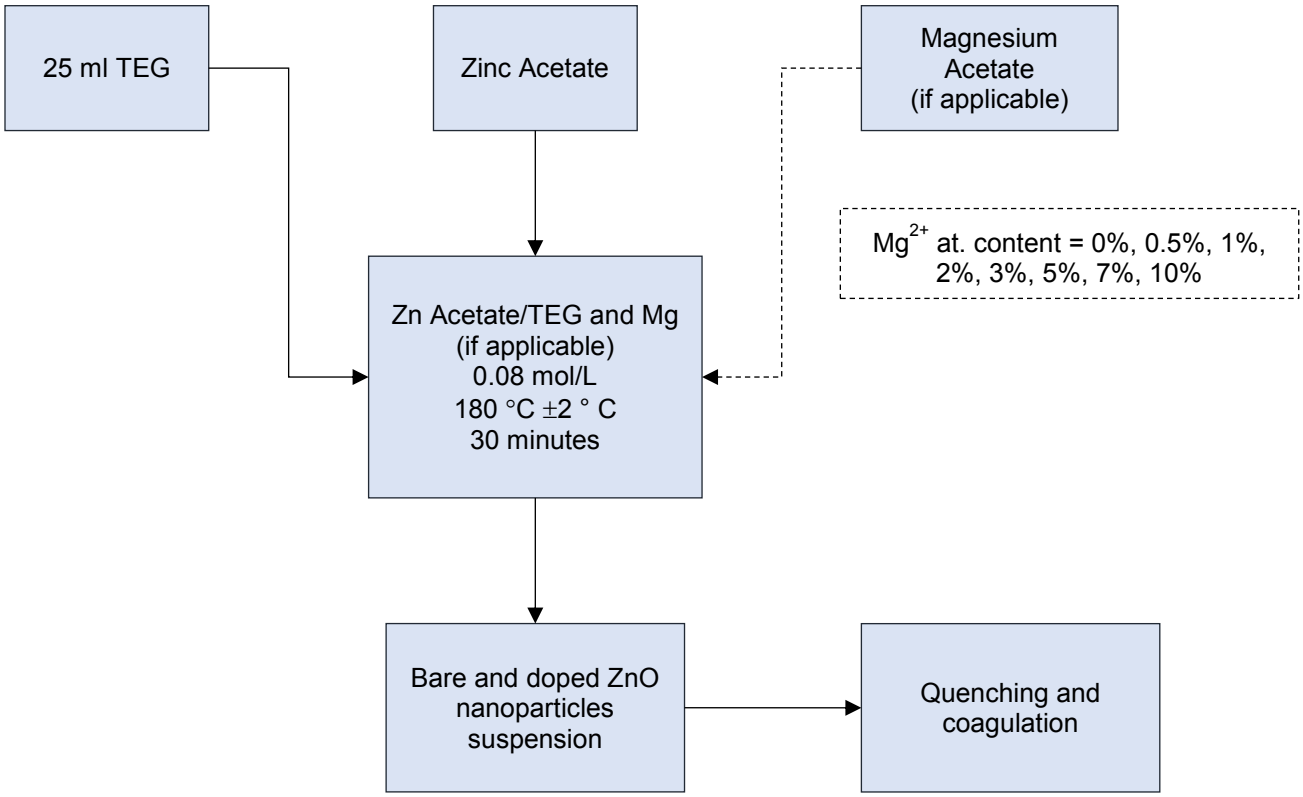

Figure 10 Synthesis of Pure and Mg-doped ZnO Nanoparticles

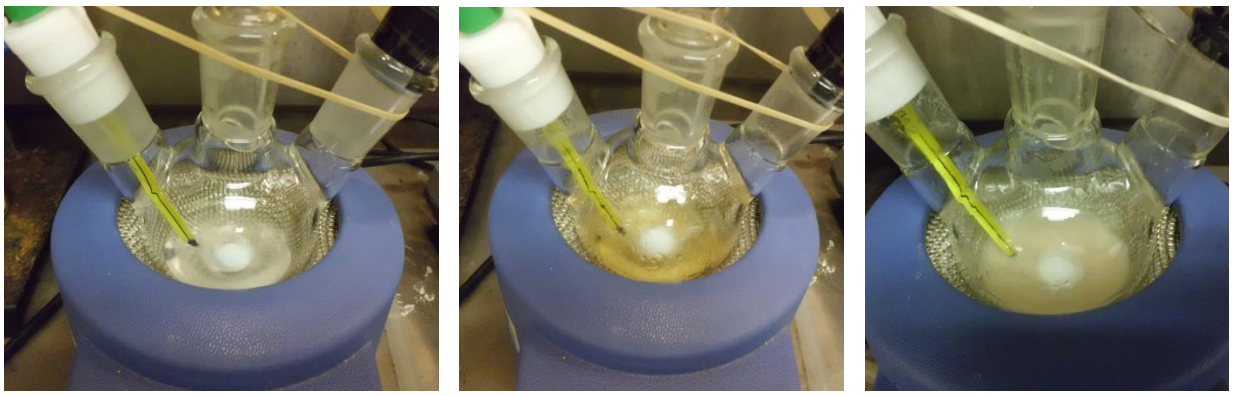

Figure 11 Experimental Setup and Reacting solutions at different times at temperature of 180 °C

3.2.2 Synthesis of chitosan/cellulose film

Figure 12 shows a scheme of the synthesis of chitosan/cellulose film via solution casting method. The cellulose w/w concentration in film was varied from 0%, 5%, 10%, 15%, 20%, 25% and 30%. Acetic acid at a concentration of 1% (v/v) was used to dissolve the chitosan, whereas N- Methylmorpholine N-oxide (NMMO) was used to dissolve the cellulose. The solutions were stirred at 1000 rpm for 4 hours at room temperature, then the chitosan solution was filtered vacuum. Required amounts of the chitosan and cellulose solutions were mixed by stirring for 1 hour and placed in a sonicator bath for 30 minutes. 20 mL of this solution were poured in a Petri dish and placed in an oven at 40 °C for 48 hours until dry. The obtained films were washed with ethanol and removed from Petry dish. Finally, to ensure that the films would dry flat, they were placed between two glass plates and dried at room temperature.

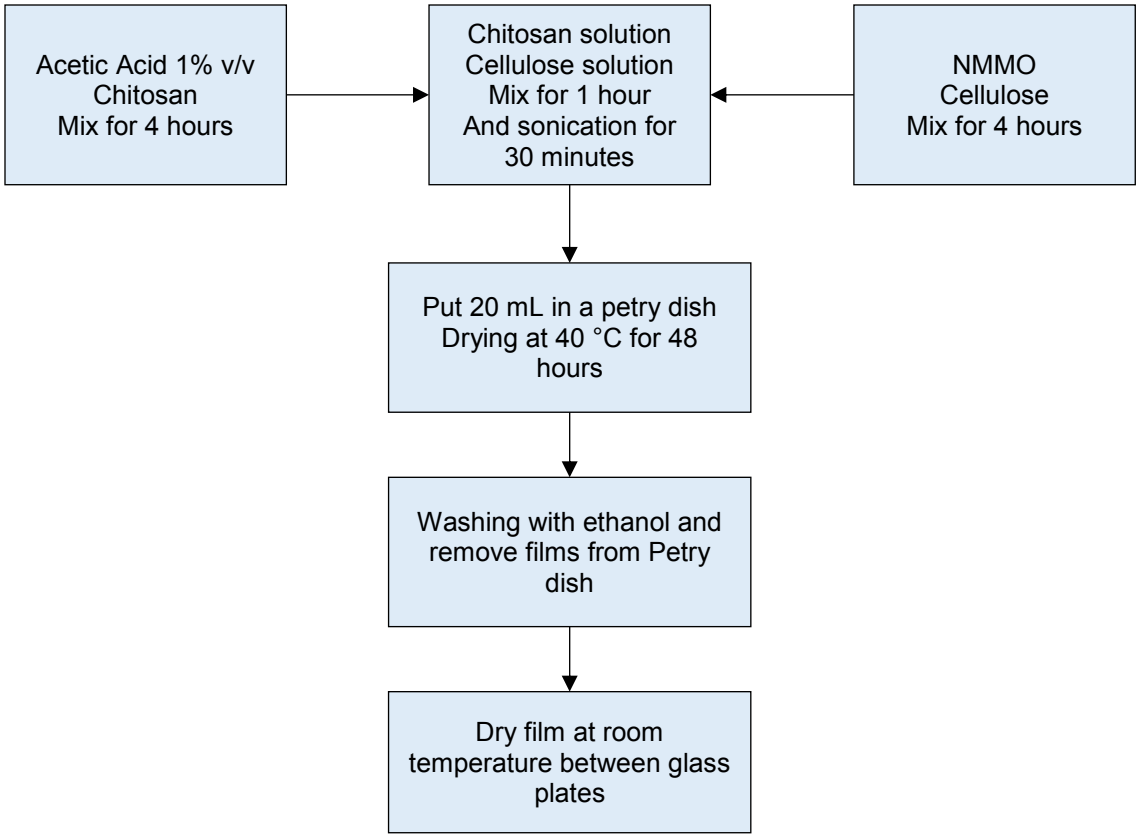

Figure 12 Synthesis of chitosan/cellulose film via solution casting method

3.2.3 Synthesis of chitosan/cellulose/ZnO nanocomposite

Figure 13 shows a scheme of the synthesis of chitosan/cellulose/ZnO nanocomposite via solution casting method. A chitosan/cellulose w/w ratio of 85/15, was set based on the observed mechanical properties in the resulting film. The nanoparticle w/w concentration in the film was varied from 0%, 1%, 3%, and 5%. The precursor powders of chitosan and cellulose were dissolved in acetic acid 1% (v/v) and NMMO respectively. The solutions were stirred at 1000 rpm for 4 hours. Coagulated and washed ZnO nanoparticles were dispersed in 1 mL of deionized water by sonication. Solutions of chitosan, cellulose and nanoparticles were mixed by stirring at 1000 rpm for 1 hour and placed in a sonicator bath for 30 minutes. This solution was poured into Petri dishes (20 mL each) and placed in an

oven at 40 °C for 48 hours until dry. The obtained films were washed with ethanol and removed from Petry dish. Finally, to ensure that the films would dry flat, they were placed between two glass plates and dried at room temperature [58]. Figure 14 shows some stages of the synthesis of nanocomposites via solution casting.

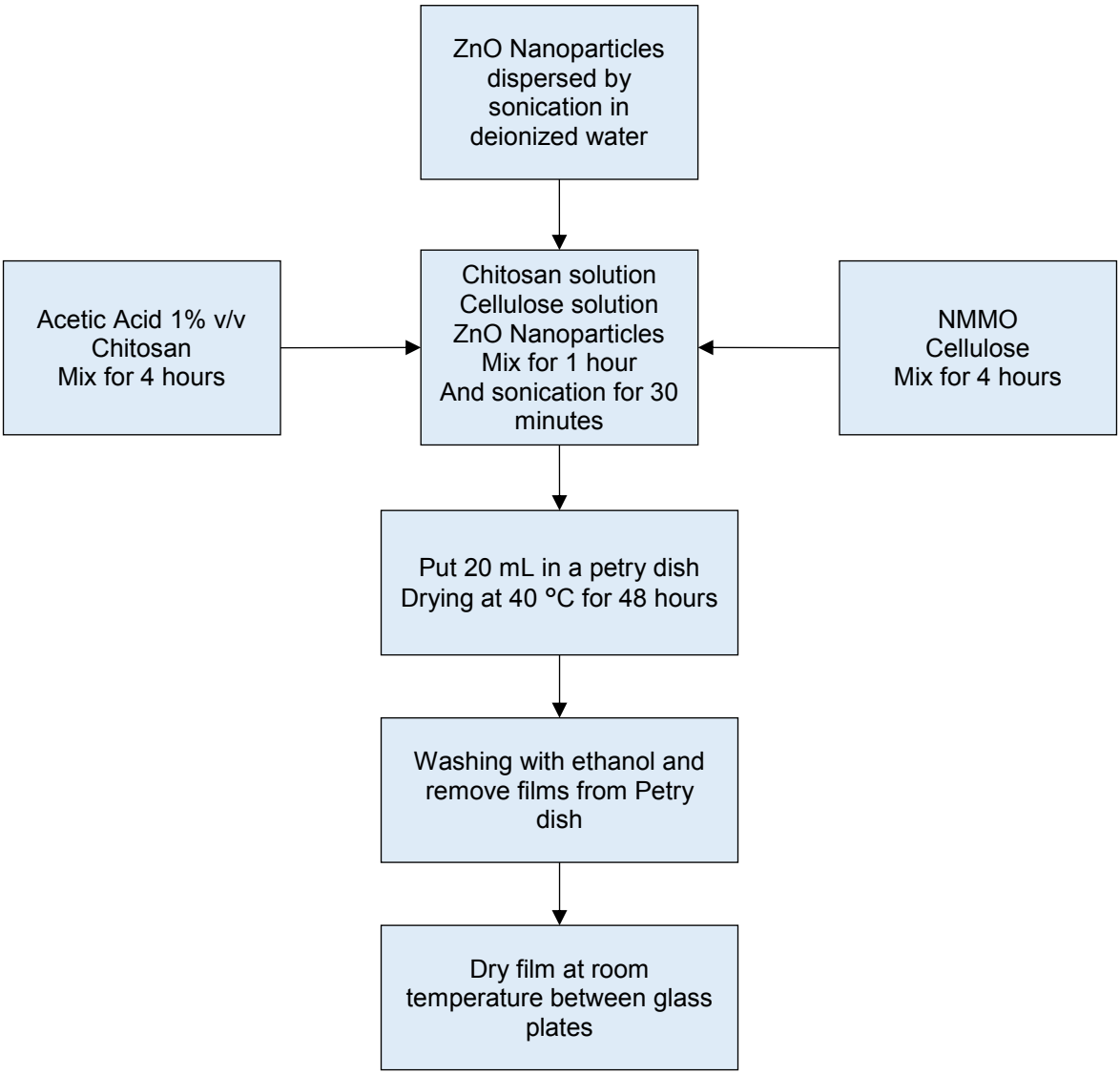

Figure 13 Synthesis of chitosan/cellulose/ZnO nanocomposite via solution casting method

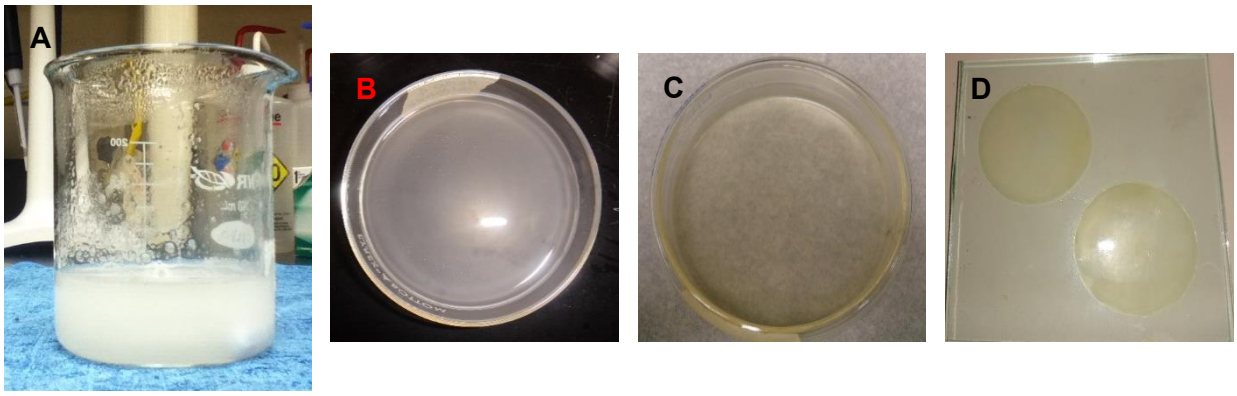

Figure 14 Synthesis of nanocomposites via solution casting. A) Suspension of ZnO nanoparticles in chitosan-cellulose precursor B) Chitosan-cellulose precursor solution in Petri dish before drying. C) Film obtained after drying at 40°C. D) Drying of films at room temperature

3.3 Materials characterization

3.3.1 Nanoparticles Characterization

3.3.1.1 X-ray Diffractometry

X ray diffraction is an analytical technique used for crystalline materials identification; the spectra provide information about crystallinity, grain size and phase composition. In this technique, the X-ray generated by a cathode ray tube, are filtered to produce a monochromatic radiation, collimated to concentrate and directed toward sample. The emitted X rays interacts with the sample producing constructive interference, the diffracted beam is sensed by the detector [60].

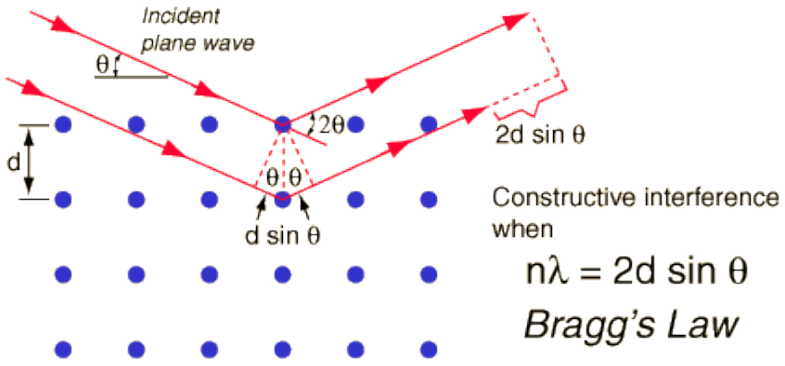

Figure 15 Scheme of diffraction and Bragg's Law [61]

This phenomena is explained by Bragg's law (Figure 15). This law describes the angle ($2\Theta_{hkl}$) formed by the incident beam and the diffracted beams and relates the wavelength of electromagnetic radiation to the diffraction angle and the lattice spacing in a crystalline sample. This equation has the form:

$$n\lambda = 2d_{hkl}\, sin\, \theta_{hkl} \quad \textit{Equation 1}$$

Where: λ is the wavelength of the incident radiation, d_{hkl} is an interplanar spacing and Θ is the diffraction angle. Diffracted electrons are used to determine crystallographic information about the sample such as crystal structure. The average crystal size may be determined using Scherrer's equation (shown below) which is derived from Bragg's law:

$$\tau = \frac{K\lambda}{\beta\, cos\, \theta} \quad \textit{Equation 2}$$

Where: K is the shape factor, usually set as 0.9

λ = is the X- ray wavelength, is this case the average Cu Kα wavelength is 0.154 nm

β = is the width of the peak at the half of the maximum intensity (FWHM), of the broadened diffraction line on the 2Θ scale in radians.

Θ = is te Bragg angle in radians

In our case the synthesized zinc oxide possesses a hexagonal structure, the lattice parameters a, and c can be determined clearing the following equation:

$$\frac{1}{d^2} = \frac{4}{3}\left(\frac{h^2+hk+k^2}{a^2}\right) + \frac{l^2}{c^2}$$ *Equation 3*

Where: *h*, *k*, and *l* are the Miller Indexes of the selected planes, *d* is the interplanar distance

The XRD analysis of pure and Mg doped ZnO nanoparticles was performed in a Siemens D5000 powder X-Ray Diffractometer with Cu Kα radiation located at the Engineering Science and Materials Department at UPRM (Figure 16). All spectra were taken from 15° to 75° and a step of 0.02.

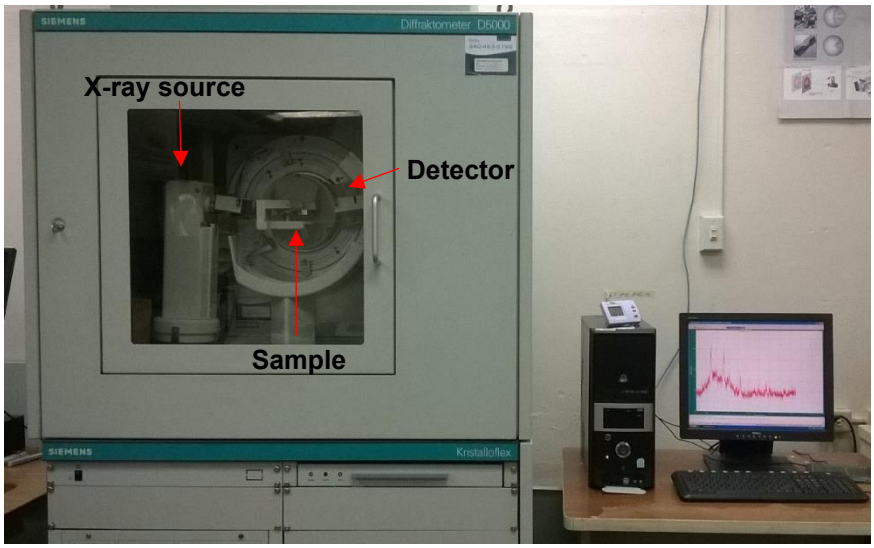

Figure 16 Siemens D5000 powder X-Ray Diffractometer

3.3.1.2 Fourier Transform Infrared Spectroscopy

This technique allows to study the vibration and rotation of molecules in the infrared region of the electromagnetic spectrum and provides information about the chemical bonding in a material, so can be used to identify a compound or analyze the composition of a sample. It is based on the fact that chemical bonds have a specific vibration frequencies which correspond to energy levels of the molecules.

The goal of the basic infrared experiment is to determine changes in the intensity of the beam of infrared radiation as a function of wavelength or frequency (2.5 – 50 μm or 4000 – 200 cm^{-1} respectively) after it interacts with the sample. The infrared spectrum is commonly plotted in three formats: transmittance, reflectance or absorbance. The samples analysis may be performed using transmittance or attenuated total reflectance (ATR).

The FTIR analysis of our samples were performed in a Shimadzu IRAffinity-1 Infrared Spectrophotometer located at the Engineering Science and Materials Department at UPRM (Figure 17). All samples were analyzed in ATR mode, in which the beam from the source reflects off of the sample and passes to the detector, thereby taking the spectra from the surface of the sample. All spectra were taken in the spectral range of 4000 - 400 cm^{-1} by accumulation of 200 scans at resolution of 4 cm^{-1}.

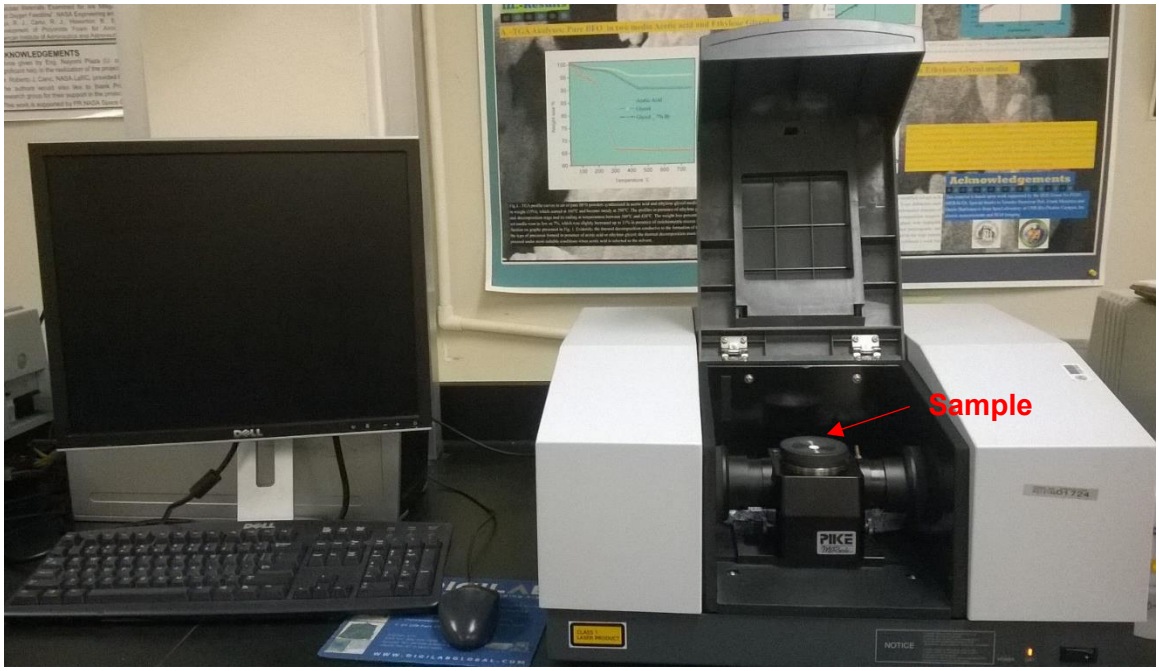

Figure 17 Shimadzu IRAffinity-1 Infrared Spectrophotometer

3.3.1.3 Optical characterization: Ultraviolet Visible Spectroscopy and Photoluminescence Spectroscopy

Transmission, reflection and absorption are optical phenomena that occur when solid crystals are irradiated by light. The absorption is the annihilation of light (photon) coming out after an electronic excitation or lattice excitation in crystals. When the electrons in a material are excited to higher energy levels, they return to their initial state by releasing the excitation energy in the form of light emission (Photoluminescence) or lattice vibrations (phonons). The Photoluminescence is the result of the absorption of a photon that generates an electron-hole pairs and produces emission of a photon of a different wavelength.

Ultraviolet and visible radiation interacts with matter, which causes electronic transitions. In the UV Vis Spectroscopy, the absorption measures transitions from the ground state to the excited state while in the Photoluminescence Spectroscopy, the fluorescence deals with transitions from the excited state to the ground state. So, this techniques are complementary.

The optical properties of pure and Mg doped ZnO nanoparticles were studied using a UV-Vis Beckman Coulter DU 800 spectrophotometer (Figure 18) and a Shimadzu RF- 5301 Spectrofluorophotometer (Figure 19) located at the Engineering Science and Materials Department at UPRM. The photoluminescense measurements were performed using an excitation wavelength of 345 nm.

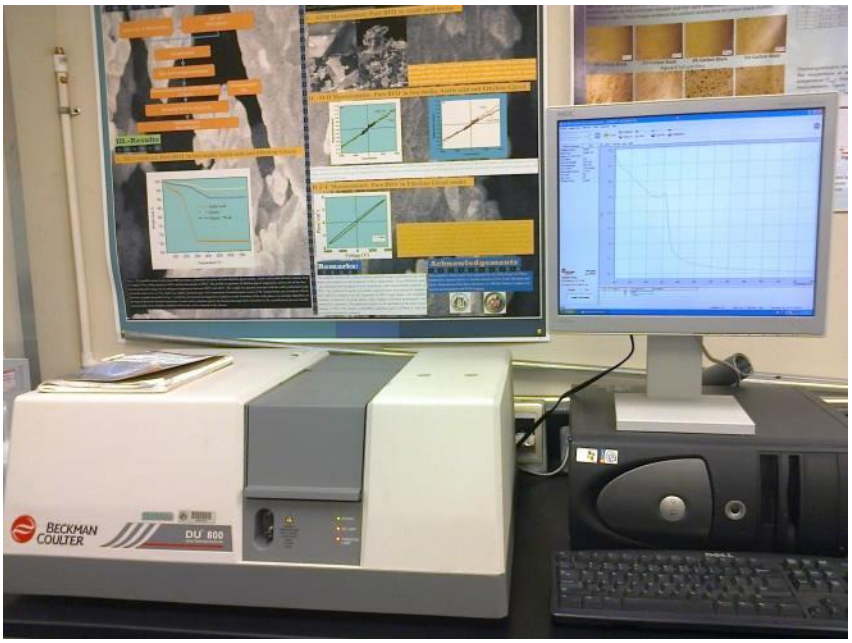

Figure 18 UV-Vis Beckman Coulter DU 800 spectrophotometer

Figure 19 Shimadzu RF- 5301 Spectrofluorophotometer

3.3.2 Films and Nanocomposite Characterization

3.3.2.1 Fourier Transform Infrared Spectroscopy

The FTIR analysis of our samples were performed in a Shimadzu IRAffinity-1 Infrared Spectrophotometer located at the Engineering Science and Materials Department at UPRM. All spectra were taken in the spectral range of 4000 - 400 cm^{-1} by accumulation of 200 scans at resolution of 4 cm^{-1} in ATR mode.

3.3.2.2 Optical Microscopy

An optical microscope provides morphological sample information by creating a magnified image of the same. This microscopy uses visible light and a system of lenses (refractive glass or quartz lenses) to magnify images of small samples. The image from an optical microscope can be captured by normal light-sensitive cameras to generate a micrograph. Modern models have a charge-coupled device cameras to capture of digital images and show the resulting image on a computer screen.

In this work the images were taken at a magnification of 10x with a Nikon Epishot 200 microscope located at the Engineering Science and Materials Department at UPRM.

3.3.2.3 Tensile test

Also known as tension test, is a fundamental materials science test, in which a sample is pulled until it breaks. It allows determine how the material will react to forces being applied in tension. In this process, the sample is places in the testing machine (universal testing machine) and slowly extending it until it fractures, the resulting graph shows how the material reacts to the force applied, the point of failure is very important and is called Ultimate Tensile Strength or UTS.

The elongation measurement is used to calculate the strain ε.

$$\varepsilon = \frac{\Delta L}{L_0} = \frac{L - L_0}{L_0}$$ *Equation 4*

Where ΔL is the change in gauge length, L_0 is the initial gauge length, and L is the final length.

The force measurement is used to calculate the stress σ.

$$\sigma = \frac{F_n}{A}$$ *Equation 5*

Where F_n is the tensile force and A is the nominal cross-section of the specimen.

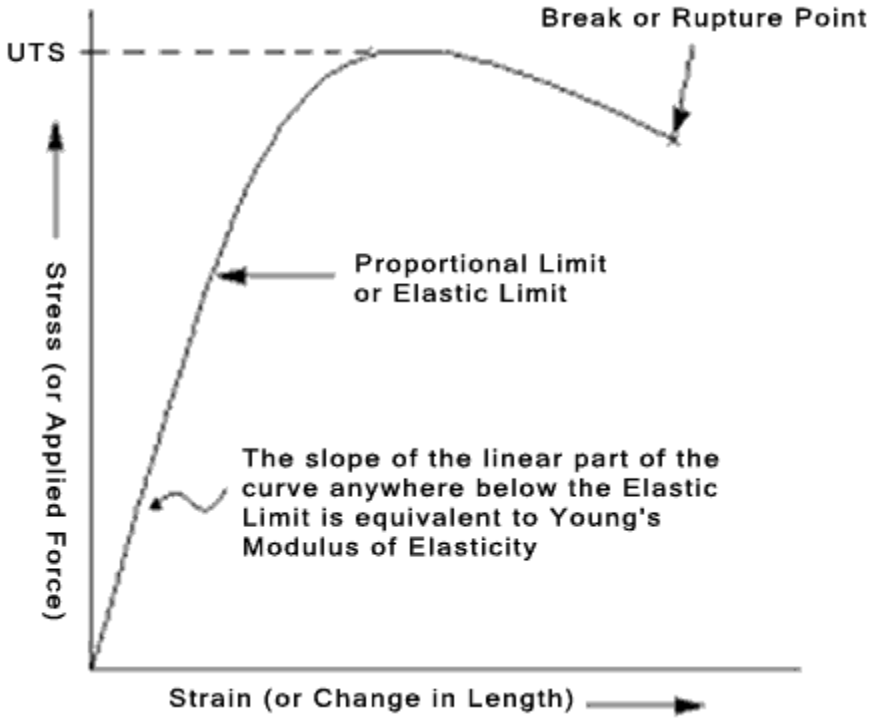

Figure 20 Stress–Strain curve [62]

The data points can be graphed into a stress–strain curve (Figure 20). For the most tensile testing of materials, the initial portion of the graph is linear and the line obeys the Hooke's Law where the ratio of stress to strain is a constant $E = \frac{\sigma}{\varepsilon}$. E is called the Modulus of Elasticity or Young's Modulus and is the slope of the line in this region.

The linear region of the graph is the elastic zone and the material will return to its original condition if the load were removed. The point at which the curve is no longer linear is called elastic, or proportional limit. From this point, the material reacts plastically and it will not return to its original, unstressed condition if the load were removed.

An Instron® (Norwood, MA, USA) model 5944 (Figure 21 A) at 1 mm/min head speed system was used to assess the tensile properties of bare and ZnO-bearing

nanocomposites. The samples tested had a dog bone shape (Figure 21 B) and were cut with a die, based on the ASTM D 1708-02a.

A Positector 6000 coating thickness gage (Figure 21 C) was used to measure the films' thickness. This electronic instrument allows realize nondestructive measurements of coating thickness applied to metals quite quickly and precision.

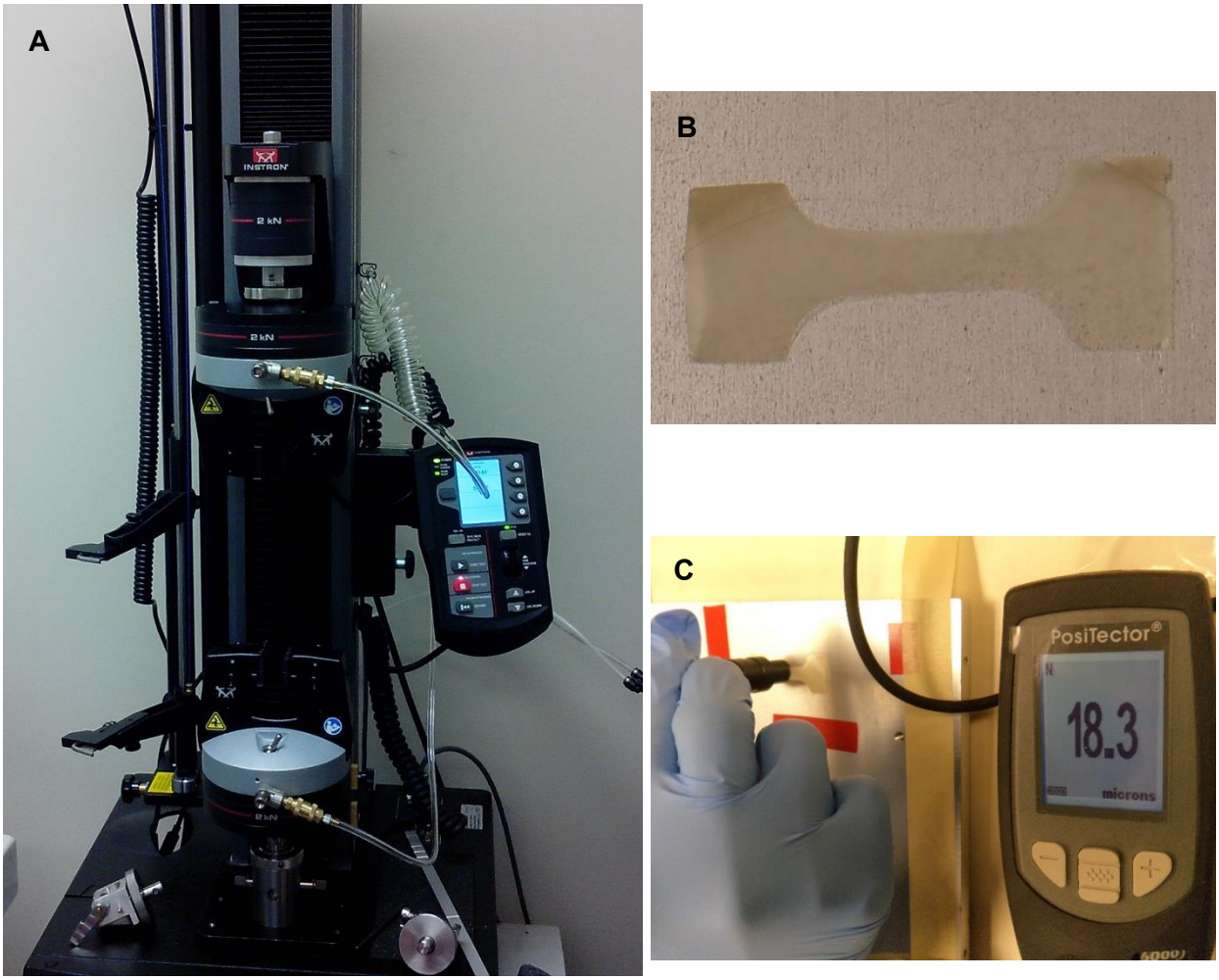

Figure 21 Tensile test. A) Instron® (Norwood, MA, USA) model 5944 - The NANOmaterials Processing Laboratory at UPRM. B) Dog bone shaped samples tested. C) Measurements of films thickness using a Positector 6000 coating thickness gage

3.3.2.4 Water vapor Permeability.

One of the most important properties of packaging materials is permeability, which can be defined as the ability to let pass substances (gases, vapors flavors) through its structure.

The ASTM E96/E96M-13 protocol allows the evaluation of the water vapor transmission by two basic methods, the desiccant method and the water method. In the desiccant method, the test sample is sealed to the open mouth of a vessel containing a desiccant, then is placed in a controlled atmosphere, the assembly is weighed periodically. In the water method, the vessel containing distilled water.

The water vapor transmission (WVT) can be calculated with the following equation:

$$WPT = \frac{G}{tA} = \left(\frac{G}{t}\right) A \quad \textit{Equation 6}$$

Where: G is the weight change, t is the time during which G occurred, G/t is the slope of straight line, and A is the test area.

The permeance is the moisture transmission rate of the material, is a performance evaluation and not a property of material, can be calculated using the following equation:

$$permeance = \frac{WVT}{\Delta p} = \frac{WVT}{S(R_1 - R_2)} \quad \textit{Equation 7}$$

Where: WVT is the rate of water vapor transmission, Δp is the vapor pressure difference, S is the saturation vapor pressure at test temperature, R_1 is the relative humidity at the

source expressed as a fraction (the test chamber for desiccant method; in the dish for water method), R_2 is the relative humidity at the vapor sink expressed as a fraction.

The permeability is a property of material, it's a theoretical number calculated by the equation:

$$permeability = permeance \times thickness \quad \textit{Equation 8}$$

The water vapor Permeability of bare and ZnO-bearing nanocomposites was evaluated using the water method described in the ASTM E96/E96M-13 with some modifications. The test samples (Figure 22A) were sealed to the open mouth of a vessel containing deionized water (Figure 22B); immediately, the assembly was weighted and placed in a glove box (Figure 22C). The test was conducted at temperature of 25 ± 1 °C and a relative humidity of 50 ± 2 %. The partial pressure difference of water vapor existing on both sides of the film provides the driving force for the flow of vapor through the film. Weight loss was recorded every 24 hours for 10 days using an analytical balance with a precision of 0.0001 g. With weights obtained during the sampling time were generated graphic weight loss versus time. A linear regression is then applied to obtain the slope of each curve, which was used to calculate the permeability using the formulas described above.

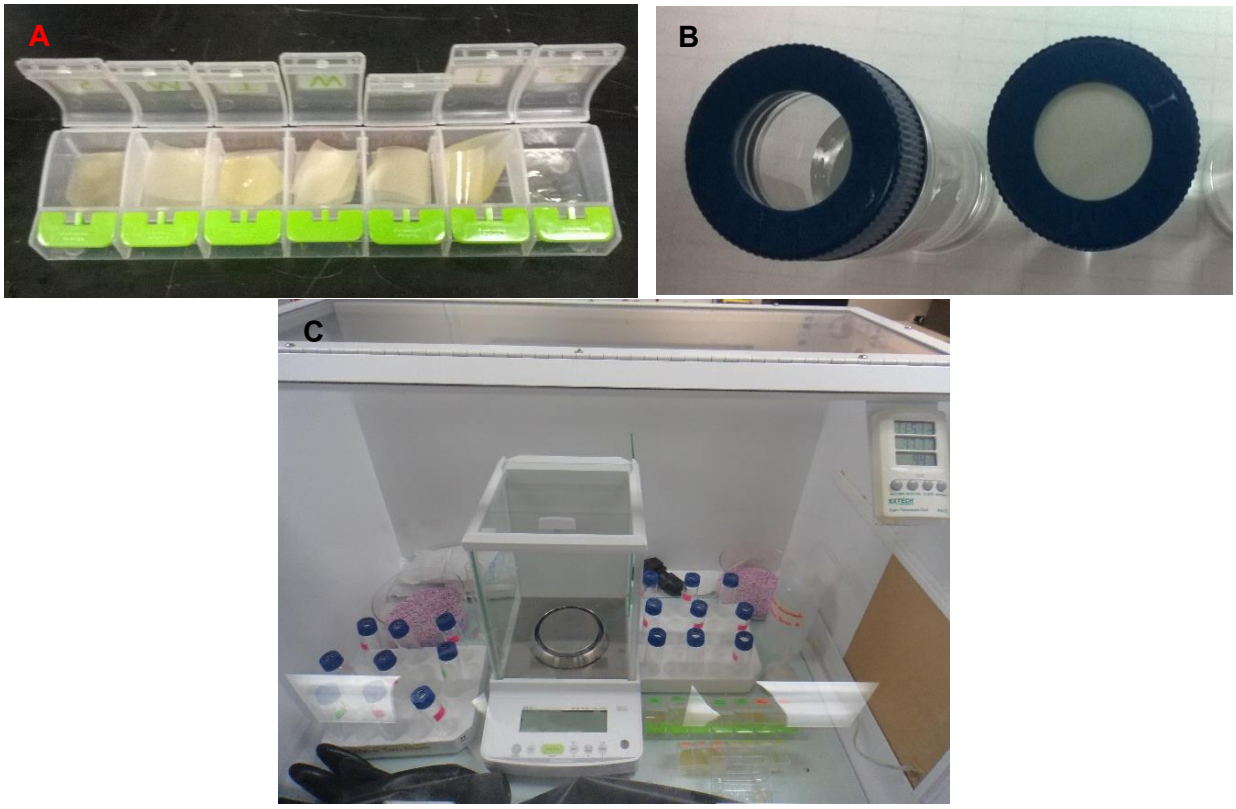

Figure 22 Assessment of water vapor permeability. A) Sample preparation, B) assembly of samples sealed to the open mouth of a vessel and a control without film, C) experimental setup

3.4 Bactericidal capacity

3.4.1 Assessment of Bactericidal capacity of Nanoparticles

The bactericidal assays of nanoparticles were performed at the Analytical Laboratory of Food, Soil and Environmental Chemistry (ALFSEC) located at the Chemistry Department – UPRM. The bactericidal capacity against *E. coli* of pure and Mg doped ZnO nanoparticles was evaluated by the Standard Plate Count Method. An Erlenmeyer flask (Figure 23B) containing 100 µL of the inoculum of E.coli (10^8 cells/mL) was mixed with 10 mL Tryptic Soy Broth (TSB) and contacted with nanoparticles at concentrations of 1000 ppm and 1500 ppm. In order to sterilize the nanoparticles, (Figure 23A), they were irradiated by ultraviolet light for 15 minutes before placing it on contact with the bacteria. A control tests (i.e., in absence of nanoparticles) was also considered.

The cultures were incubated at 37 °C and 250 rpm for 24 hours. After incubation time, the samples were submitted to serial dilutions (Figure 23D) until reach a dilution factor of 10^7. A volume of 0.1 mL from the last dilution was spreaded on MacConkey Agar plates and incubated at 37 °C for 24 hours. The colonies were quantified in order to calculate the bacterial growth inhibition (Figure 23E) using the $\%Inhibition = \frac{Colonies_{control} - Colonies_{sample}}{Colonies_{control}} \times 100$ Equation *9*. The Standard Plate Count Method was carried out two times in triplicate, for each nanoparticle concentration.

$$\%Inhibition = \frac{Colonies_{control} - Colonies_{sample}}{Colonies_{control}} \times 100 \quad \text{Equation 9}$$

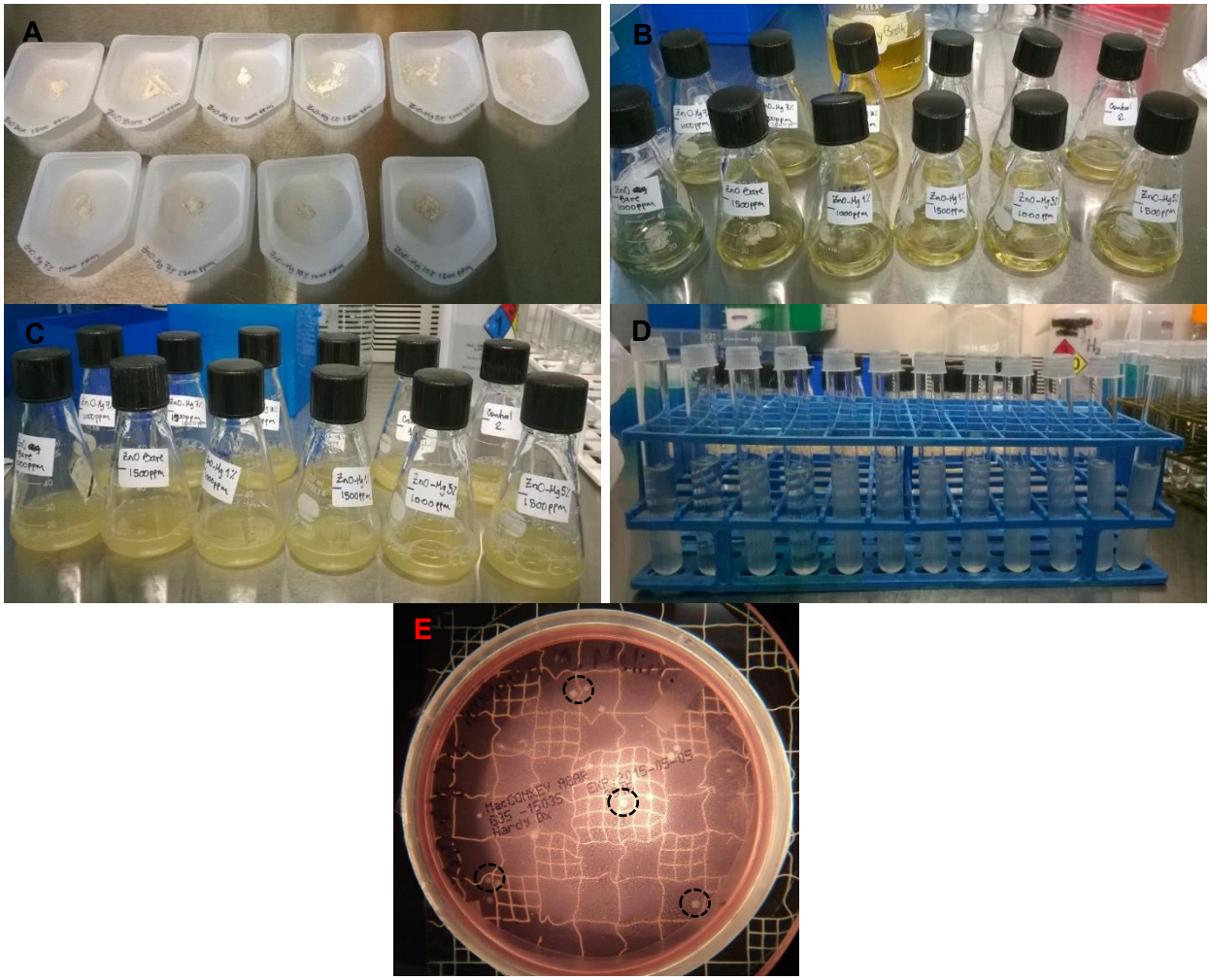

Figure 23 Assessment of bactericidal capacity. A) ZnO nanoparticles, B) Tryptic Soy Broth and nanoparticles. C) Tryptic Soy Broth, ZnO Nps and E. coli after incubation D) Serial dilutions, E) Colony counting

3.4.2 Assessment of Bactericidal capacity of nanocomposites.

The bactericidal assays of nanocomposites bearing 0, 3, 5 and 10% w/w ZnO-Mg nanoparticles were performed at the Analytical Laboratory of Food, Soil and Environmental Chemistry (ALFSEC) located at the Chemistry Department – UPRM. The bactericidal capacity against *E. coli* of bare and ZnO-bearing nanocomposites was evaluated by the Standard Plate Count Method as described above. In this case, the

nanocomposite was cut into small pieces (Figure 24A) and placed under ultraviolet light for 15 minutes (each side) before placing it on contact with the bacteria. The nanocomposite concentration was 15000 ppm. A control tests (in absence of nanocomposite) was also considered. The concentration of nanoparticles in the culture medium excluding the polymeric matrix was 0, 150, 450, 750 and 1500 ppm. The Figure 24B shows the nanocomposite in the culture medium with the inoculum before the incubation.

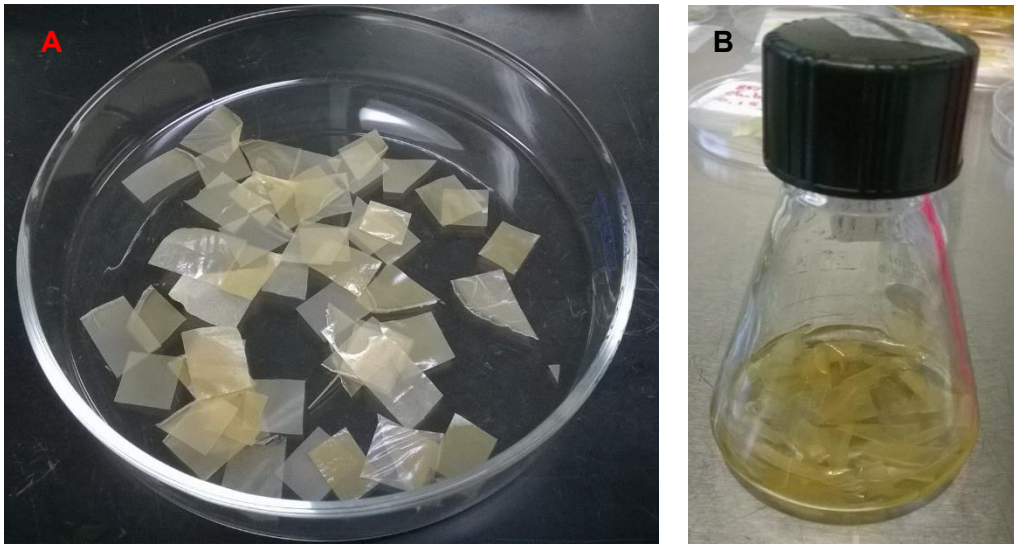

Figure 24 Assessment of nanocomposite bactericidal capacity. A) Nanocomposite cut in small pieces B) Tryptic Soy Broth and nanocomposite

3.5 Measurement of Singlet Oxygen (SO) [63][64]**.**

The generation of singlet oxygen in our samples was determined using a Singlet Oxygen Sensor Green (SOSG) reagent kit. This SOSG is highly sensitive for singlet oxygen but is not sensitive to superoxide, hydroxyl radical or other Reactive Oxygen Species (ROS). Originally the SOSG show a weak blue fluorescence but in the presence of SO exhibits a green fluorescence with excitation/emission maxima ~504/525 nm.

The main component of SOSG is 9-[2-(3-Carboxy-9,10-dimethyl)anthryl]-6-hydroxy-3H-xanthen-3-one (DMAX), which reacts rapidly with SO producing 9,10-endoperoxide (DMAX-EP). DMAX and DMAX-EP show similar excitation/emission wavelengths (492/515 nm), however DMAX does not show fluorescence while DMAX-EP is highly fluorescent in the presence of SO. The Figure 25 shows DMAX and MDAX-EP.

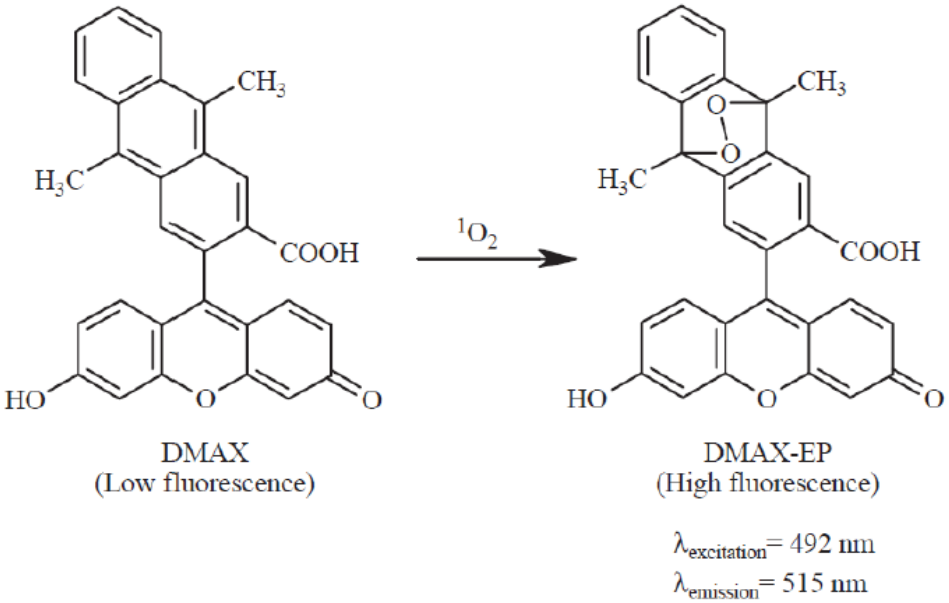

Figure 25 Reaction of 9-[2-(3-carboxy-9,10-dimethyl)anthryl]-6-hydroxy-3H-xanthen-3-one (DMAX) with SO produced by the excitation of Nanoparticles to generated DMAX-EP [64].

3.5.1 Experimental Method to determine the generation of SO.

First, a “stock solution” was prepared by dissolving 100µg (powder) of sensor green in 33µL of methanol HPLC grade ≥ 99.9% and 297 µL of deuterated water at 50%. The final concentration of DMAX was 0.5 mM. Then a blank solution (without nanoparticles) was prepared with 1447 µL of deuterated water at 50%, 3 µL of the stock solution and 50 µL of deionized water. The suspension containing the nanoparticles was prepared in the same way as the blank, the difference is that the deionized water containing suspended

nanoparticles (333.33 mg/L). A Shimadzu RF- 5301 Spectrofluorophotometer was used to determine the generation of SO species, via the following protocol:

1. 700 µL of the suspension containing the nanoparticles were withdrawn from the total suspension.
2. The PL spectra, with an excitation wavelength of 488 nm and using a slit 3-3, were recorded (T_0)
3. The suspension was excited at 345 nm (slit 5-5) for 30 seconds.
4. Steps 2 and 3 were repeated until get the spectra T_9

Other 700 µL of the suspension were withdrawn and steps 2 to 4 were repeated to get results by duplicated. This protocol was also used for the blank solution. The suspensions were excited at 345 nm because it was the excitation wavelength in the Photoluminescence measurements.

CHAPTER IV: RESULTS AND DISCUSSION

4.1 Pure and Magnesium doped ZnO Nanoparticles

4.1.1 X-ray Diffraction

Figure 26 displays the X-ray diffractograms from pure and Mg-doped ZnO nanoparticles (dopant concentration of 0, 1, 3, 5, and 10 at.% are presented in Figure 26 a), dopant concentration of 0.5, 2 and 3 at.% are shown in Figure 26 b). All peaks were assigned to ZnO-wurtzite phase; no diffraction peaks corresponding to isolated Mg-phases were detected that would suggest the actual incorporation of Mg^{2+} species (0.65 Å) into the Zn^{2+} (0.74 Å) sites. This incorporation is favored by the smaller ionic radii of Mg^{+2} compared to Zn^{+2} [4].

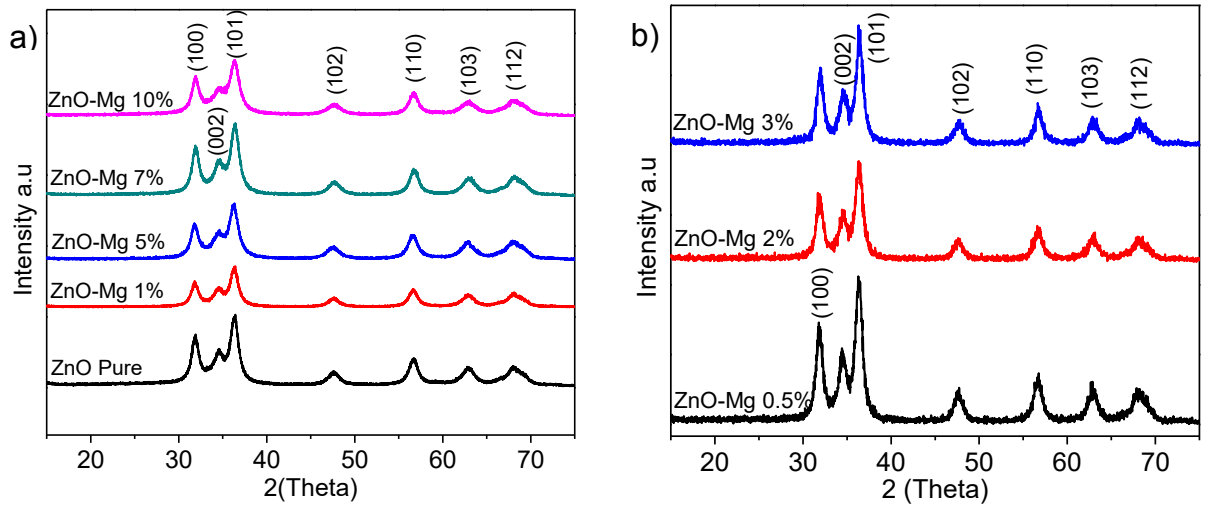

Figure 26 XRD patterns of pure and Mg-doped ZnO nanoparticles. a) Dopant concentration of 0, 1, 3, 5, and 10 at.%, b) Dopant concentration of 0.5, 2 and 3 at.%.

The average crystallite size are presented in Table 4. The reflection peaks at 2Θ = 47.6, 2Θ = 56.6 and 2Θ = 63.0 were chosen to calculate the average crystallite size for pure and Mg doped using the Scherrer's equation ($\tau = \frac{K\lambda}{\beta \cos\theta}$ Equation 2). In general, the average crystallite sizes for nanoparticles synthesized remained in the 6nm - 8nm range for all samples.

Table 4 Average crystallite size of ZnO Nanoparticles synthesized at various dopant atomic percentages

Sample	Average Crystallite Size (nm)	Standard Deviation (nm)
ZnO Puro	6.6	1.1
ZnO-Mg 0.5%	7.2	0.8
ZnO-Mg 1%	6.9	0.8
ZnO-Mg 2%	6.7	1.1
ZnO-Mg 3%	7.3	1.4
ZnO-Mg 5%	5.8	0.7
ZnO-Mg 7%	6.4	1.0
ZnO-Mg 10%	5.5	1.3

4.1.2 Fourier Transform Infrared Spectroscopy.

Figure 27 displays the FTIR spectra of pure and Mg-doped ZnO nanoparticles (dopant concentration of 0, 1, 3, 5, and 10 at.% are presented in Figure 27 a), dopant concentration of 0.5, 2 and 3 at.% are shown in Figure 27 b). A clear band centered on 536 cm^{-1} that correspond to Zn-O stretching vibration can be observed confirming the formation of the oxide [65]. The bands at 1072 cm^{-1} and 1420 cm^{-1} are associated to stretching vibration of -CO and bending vibration of -CH respectively, these band reveal the presence of absorbed by product related to the functional groups of polyol, which would have generated a net surface charge on the nanoparticles surface inhibiting their

growth and excessive aggregation. The band at 1595 cm^{-1} can be assigned to residual water on the surfaces of the samples. A band centered at 3381 cm^{-1} is attributed to O-H stretching vibration of hydroxyl group.

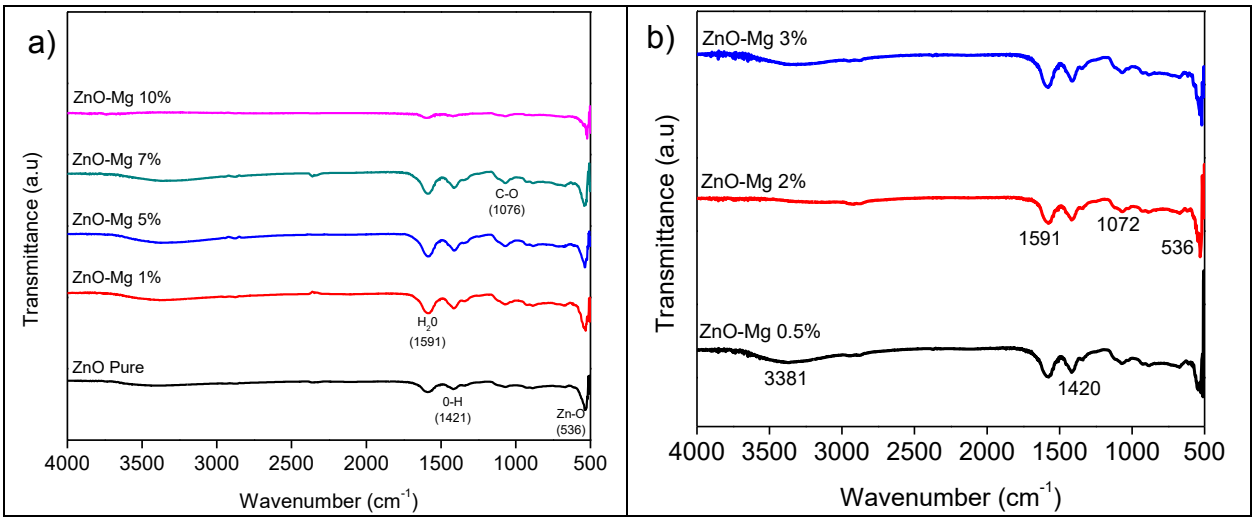

Figure 27 FTIR spectra of pure and Mg-doped ZnO nanoparticles. a) Dopant concentration of 0, 1, 3, 5, and 10 at.%, b) Dopant concentration of 0.5, 2 and 3 at.%.

4.1.3 Morphological analysis: Scanning Electron Microscopy (SEM)

Figure 28 shows Images SEM of pure (a), 0.5% (b and c) and 10% (d) Mg doped ZnO nanoparticles. Pure ZnO nanoparticles are spherical and mono dispersed with an average size around 65 nm. The difference in particle size obtained from XRD and SEM measurements suggest that final particles are poly-crystals consisting of small primary crystallites, which have an average particles size of ~ 7 nm (XRD results). The size of the final particles was also corroborated in TEM images obtained for pure zinc oxide (Figure 29 a and b). Spherical nanoparticles were obtained, with a size below 200 nm and 100 nm, for doping 0.5 at. % and 10 at. %-doped particles, respectively.

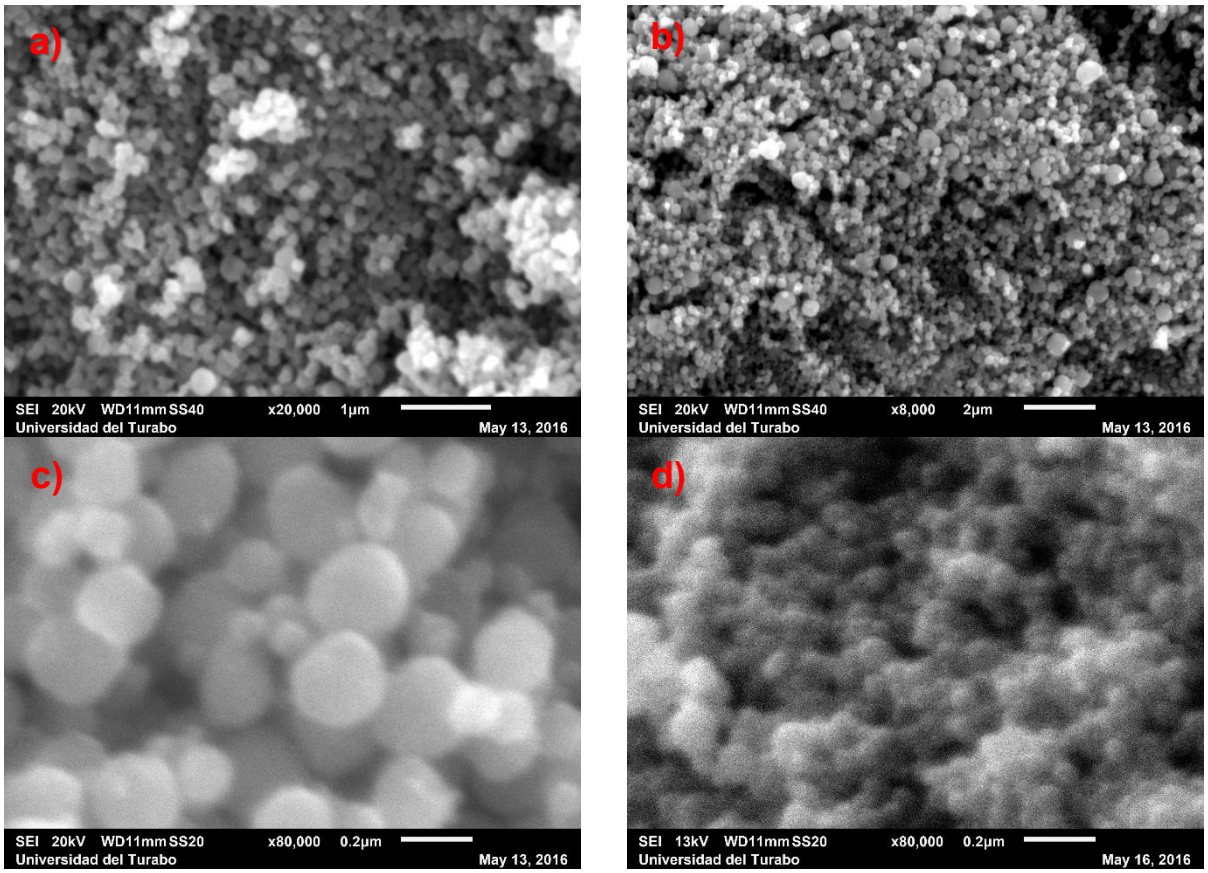

Figure 28 Images SEM of a) pure, b) 0.5% Mg, c) 0.5% Mg and d) 10% Mg doped ZnO nanoparticles - using a JEOL JSM-6010LA Scanning Electron Microscopy - located in Puerto Rico Energy Center, Universidad Del Turabo

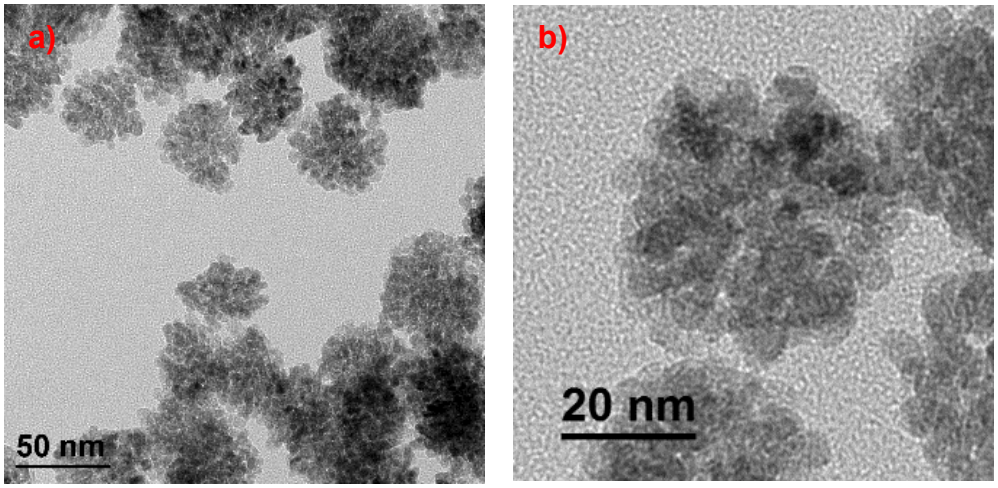

Figure 29 Images TEM of pure ZnO nanoparticles - using JEM-ARM200cF Transmission Electron Microscope located in Florida State University Research Foundation

4.1.4 Optical Properties

4.1.4.1 Absorbance (UV- Vis Spectroscopy)

Figure 30 shows the absorption spectra of pure and Mg-doped ZnO nanoparticles (dopant concentration of 0, 1, 3, 5, and 10 at.% are presented in Figure 30 a), dopant concentration of 0.5, 2 and 3 at.% are shown in Figure 30 b). When a photon is absorbed by a semiconductor (such as ZnO) an exciton can be formed, which excites an electron from the valence band to the conduction band, in turn, this leaves a positively charged electron hole.

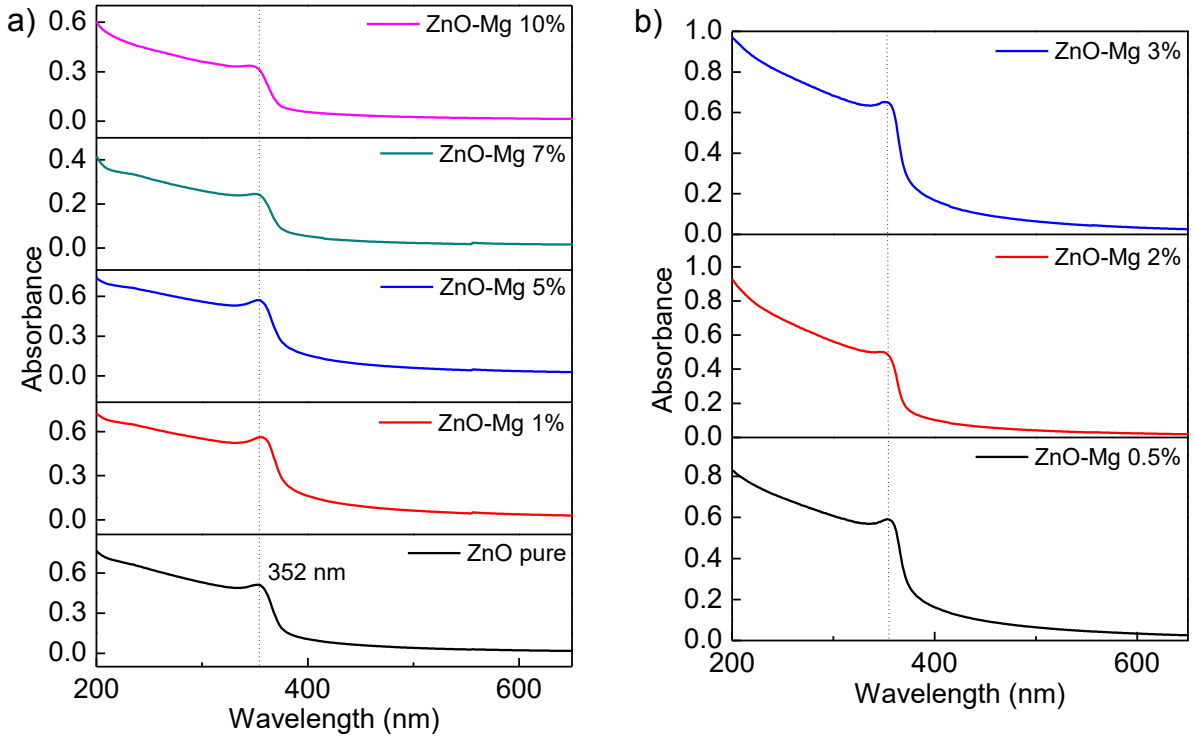

Figure 30 UV-vis spectra of pure and Mg doped ZnO nanoparticles. a) Dopant concentration of 0, 1, 3, 5, and 10 at.%, b) Dopant concentration of 0.5, 2 and 3 at.%.

In the case of ZnO pure, the corresponding exciton peak is centered on 352 nm. For the nanoparticles synthesized at different concentration of Mg^{2+} dopant the exciton shoulder exhibits a negligible shift (Table 5). This could be related to the similarity in the crystal size (between 6nm - 8nm). These results are agreement with the XRD measurements.

The materials have energy bands. The valence bands is the low energy states and is occupied by electrons. In turn, the conduction bands has high energy and are not occupied by electrons. The region between the top of valence band and the bottom of conduction band is known as band gap.

The band gap energy of pure and Mg-doped ZnO nanoparticles was estimated using Tauc's relationships, by extrapolation of the linear portion of $(\alpha h\upsilon)^2$ versus $(h\upsilon)$ plots [66]. Figure 31 and Table 5 show the estimated band gap of synthesized nanoparticles; all estimated values were very similar and varied between 3.30 to 3.34 eV. The aggregation of particles makes these optically behave like ZnO bulk that exhibit a band gap energy of 3.3 eV [17].

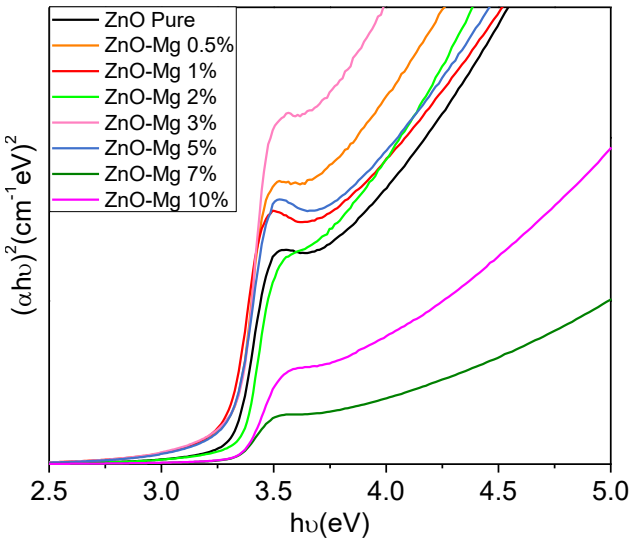

Figure 31 Optical Band Gap determination for pure and Mg doped ZnO nanoparticles

Table 5 Exciton peak position and Optical Band Gap determinate of ZnO Nanoparticles synthesized at different concentration of Mg^{2+} dopant

Sample	exciton peak position (Wavelength (nm))	Band Gap energy (eV)
ZnO pure	352	3.32
ZnO-Mg 0.5%	354	3.31
ZnO-Mg 1%	355	3.30
ZnO-Mg 2%	351	3.33
ZnO-Mg 3%	352	3.31
ZnO-Mg 5%	354	3.31
ZnO-Mg 7%	349	3.34
ZnO-Mg 10%	348	3.34

One of the advantages that zinc oxide can provide to a polymeric matrix is the absorption of Ultra Violet light [22]. This property is very important for food packaging industry, since the quality of some food product is deteriorated by the light. Plastic films are generally transparent to UV and visible radiation of short wavelength. Therefore the addition of ZnO nanoparticles could provide protection to food products light sensitive such as fruits, vegetables, vitamins, among other [67].

4.1.4.2 Photoluminescence (PL) Measurements

Figure 32 presents the PL spectra of pure and Mg-doped ZnO nanoparticles. (Dopant concentration of 0, 1, 3, 5, and 10 at.% are displayed in Figure 32 a), Dopant concentration of 0.5, 2 and 3 at.% are shown in Figure 32 b). The spectrum of pure ZnO nanoparticles shows UV and visible peaks at 362 nm and 390 nm respectively. The emission band at 362 nm is attributed to the recombination of electron-holes pairs; the violet emission band at 390 nm is associated to zinc interstitials and the transition of

electron from donor level near conduction band to the valence band [65][57][68]. For all the Mg^{2+} doped samples, we can observed the same emissions bands.

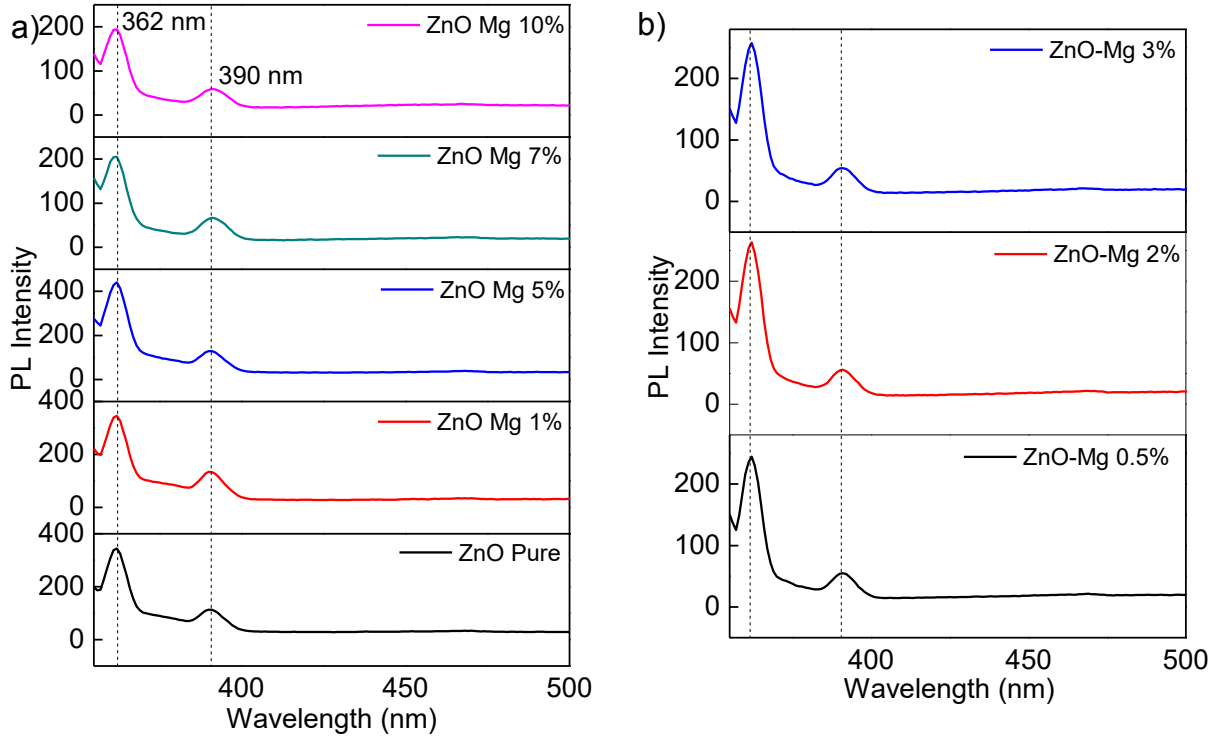

Figure 32 PL spectra of pure and Mg doped ZnO nanoparticles. a) Dopant concentration of 0, 1, 3, 5, and 10 at.%, b) Dopant concentration of 0.5, 2 and 3 at.%.

For the emission at 362 nm, the synthesized samples (except ZnO-Mg 5%) shown a quenching effect by concentration; this occurs when the non-radiative transitions are higher than the emission due to the high dopant concentration.

Fresh produce and meats spoiled, exhibit smells and colors easy to distinguish by consumers. Some packaging materials do not allow appreciate the sensory characteristics of food containing, by which the consumer rely on sell-by dates which are determined by the manufacturer taking into account the conditions of storage and

transport suitable for the product, this sell- by dates could not apply if the food is not stored and transported at suitable temperature [20].

The optical properties of nanoparticles could provide solutions to this problem because through them could detect the presence of gases, chemical contaminants and pathogens. Some of the tests are based on the observed color changes and other are dependent on fluorescence (used for small molecules). Some bacterial toxins have been detected using antibody-labeled luminescent quantum dots, which could be used in food safety [20]. In this sense the photoluminescence of the nanoparticles of zinc oxide could probably be used as sensor of gas, pathogens and other contaminants.

4.1.5 Bactericidal capacity against *E. coli*.

The bactericidal assay was carried out by colony count method, after completing seven successive dilutions, the last dilution seeded on Mac Conkey Agar plates (more details in section 3.4.1). In *Figure 33* (a) and (b), typical *E. coli* colonies, pink, with a circular morphology, convex surface and rounded edges, can be observed. These images correspond to the growth of *E coli* after 24 hours of incubation of control sample without nanoparticles and with 1000 ppm of Mg- ZnO 1% nanoparticles respectively. We can see that plate corresponding to concentration of 1000 ppm of Mg-ZnO 1% has fewer colonies, compared to the control sample, which indicates that there was inhibition of bacterial growth.

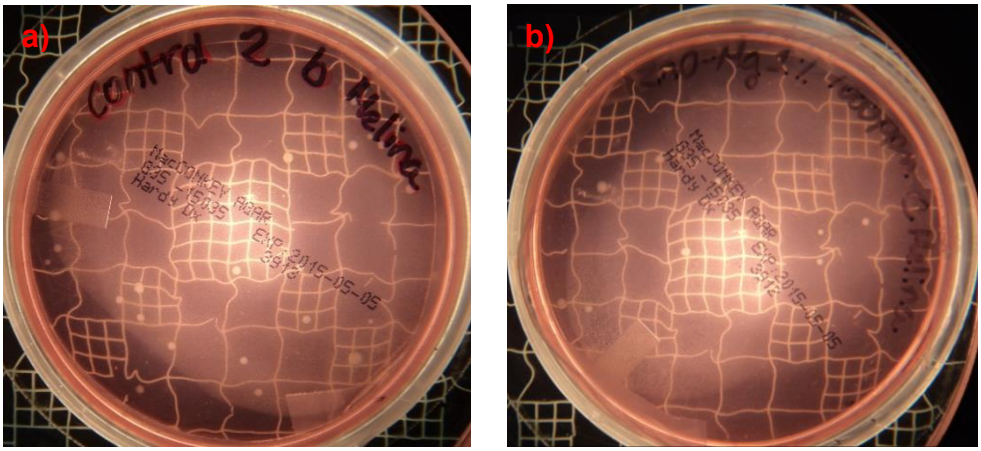

Figure 33 E. coli colonies on Mac Conkey agar plates; a) control without nanoparticles and; b) assays for 1000 ppm of Mg- ZnO 1% nanoparticles

Figure 34 shows the variation of the percentage of *E. coli* inhibition at different concentrations of Mg doping and Mg-ZnO nano pure and Mg doped ZnO nanoparticles. As the data in this figure suggests, the incorporation of Mg up to 1% (at 1000 ppm of particles concentration) would enhance the bactericidal capacity, compared to pure ZnO. It can be explained by the formation of Zn-Mg solid solution, in which Mg species could have replaced Zn sites in the ZnO host lattice and reinforced the bactericide capacity of Zn species (it is known that MgO can also exhibit good bactericidal capacity [29][69]). However, for a Mg doping level above 1%, the inhibition went down drastically which may be due to the potential precipitation of an isolated and poorly crystalline Mg compound, due to the partial substitution of Zn by Mg atoms in the host lattice. At high particles concentration (1500 ppm), all samples exhibited bactericidal capacity against *E. coli*. However, the growth inhibition capacity trends to decrease with increase of the dopant concentration. This decrease is more noticeable for Mg doping levels above 5%, which could be attributed to the increase of the amount of the Mg isolated compound mentioned earlier.

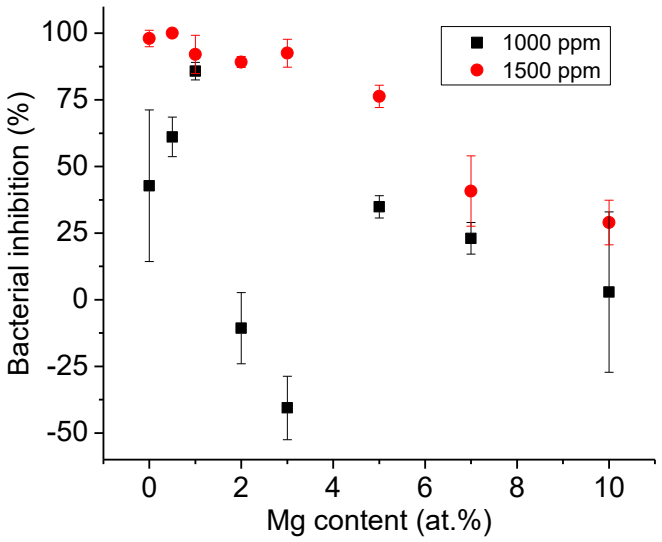

Figure 34 Bacterial inhibition of E. coli in presence of: pure and Mg doped ZnO nanoparticles. The bacteria were contacted with 1000 and 1500 ppm of powdered samples in each case.

The ANOVA-two factor is presented in Table 6. A P- value of 0.0111 was determined for the nanoparticles concentration in the culture medium, which indicates that this factor has a statistically significant effect in bacterial inhibition. At the same time, a P- value of 0.2891 for doping level, shows that this factor has no significant effect; in other words, the enhancement of the bactericidal effect will be more influenced by the particles concentration rather than the doping level in the ZnO particles.

Table 6 ANOVA two factor for bacterial percentage for E. coli in presence of pure and Mg doped ZnO nanoparticles.

Source of Variation	***SS***	***df***	***MS***	***F***	***P-value***	***F crit***
Mg 2+ Content (at. %)	10141.85	7	1448.84	1.5483	0.2891	3.7870
Nps Concentration (ppm)	10959.65	1	10959.65	11.7119	0.0111	5.5914
Error	6550.42	7	935.77			
Total	27651.92	15				

In order to select the best nanoparticle for later use in the nanocomposite it was decided to perform an additional test using a particle concentration of 1200 ppm and three different doping levels: 0, 0.5 and 1 at.% Mg. These results can be seen in Figure 35.

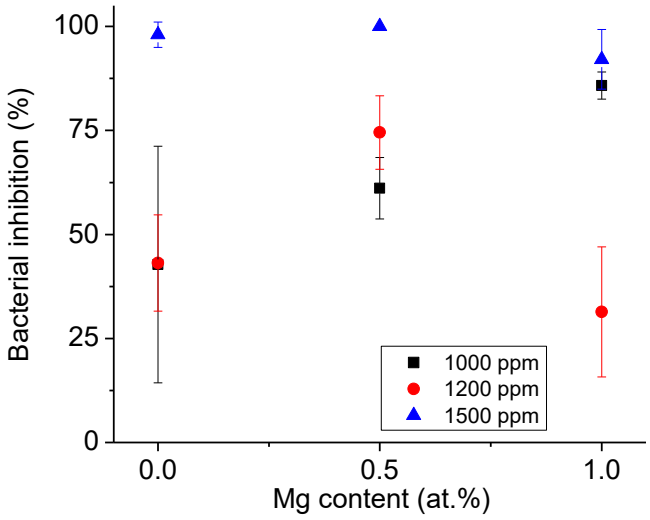

Figure 35 Bacterial inhibition for E. coli in presence of: pure, and Mg doped 0.5 and 1 at. % ZnO nanoparticles.

On a general basis, the Mg doping exhibited a positive effect on the inhibition growth at 0.5 at. %. Accordingly, this doping level was selected to be dispersed within the polymer matrix of chitosan and cellulose. The corresponding results will be shown in section 4.3.

In some cases a high variability was obtained, which can be explained due to the method used, because sometimes the colonies grow together in chains or groups making it difficult to count, which generates differences in the number of colonies counted on each replica. These variations could be minimized by increasing the amount of data collected;

in our case, the bactericidal tests were performed two times in triplicate for each concentration of nanoparticles.

4.1.5.1 Generation of Singlet Oxygen species

In general, the bactericidal capacity of the Zinc oxide nanoparticles can be attributed to the generation of Reactive Oxygen Species such as OH^-, H_2O_2 [13][18]. Is important to mention that the synthesized nanoparticles can produce singlet oxygen species, as evidence by complementary analyses. As was described in the experimental section 3.5, the generation of singlet oxygen was determined using a Singlet Oxygen Sensor Green (SOSG) kit. The SOGS is highly fluorescent in presence of SO at 525nm. The Figure 36 shows the fluorescence spectra of the suspension containing SOSG with and without nanoparticles of different dopant concentration. In this graph we can see clearly the increase in the PL intensity at 525 nm with the increase of UV exposure time, indicating a large generation of SO.

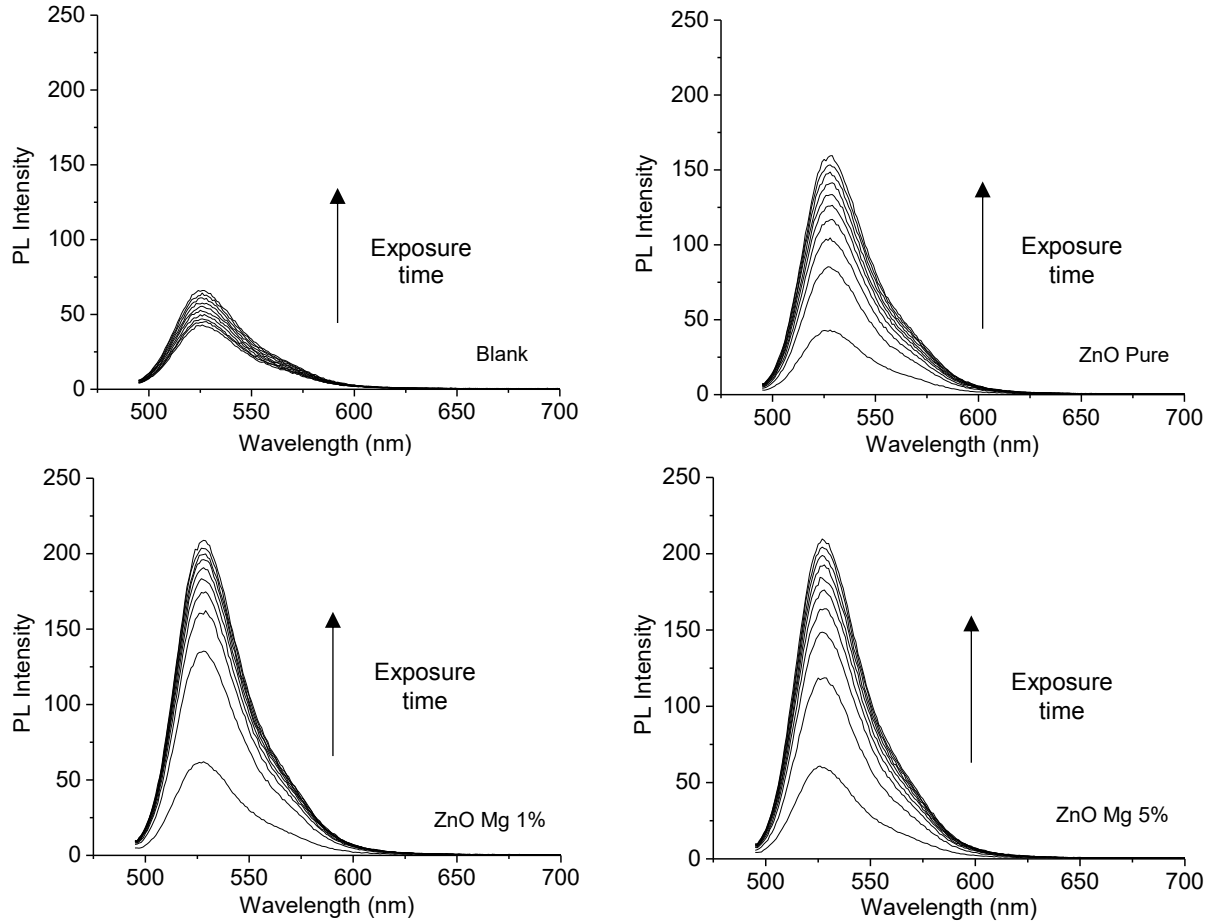

Figure 36 PL spectra of the 525nm emission peak associated to the generation of SO species. The excitation wavelength was 345nm [59]

In order to visualize better the effect of Mg^{2+} in the generation of singlet oxygen, Figure 37 present the evolution of the PL intensity at 525 nm as a function of the UV-irradiation time of the blank solution (only sensor green) and the suspension bearing pure and Mg -doped ZnO nanoparticles at different doping levels in the 0 at.%-10 at. % range. Evidently, all the ZnO nanoparticles (pure and doped) in the 1 at.%-7 at. % Mg range generated more SO when compared to the blank solution, this solution not containing nanoparticles, so there is no generation of singlet oxygen and consequently an increase in the intensity of 525 is not evident; however, the sample with Mg-doped 1 at. % was the most effective, this can be explained in terms of the nanocrystal quality; in this case, we could suggest

that the Mg incorporation generated more defects in the particle so there is more electrons available to produce redox reaction that leads to the SO production. For the sample with Mg-doped 10 at.% decreases the yield compared to blank. These results are in agreement with those obtained in the bactericidal assay, in which, for a doping level above 1 at. % the potential precipitation of an isolated Mg compound due to the substitution partial of Zn by Mg atoms have a negative effect in the bactericidal properties. Similarly, we might suggest that this Mg compound interferes with the singlet oxygen generation.

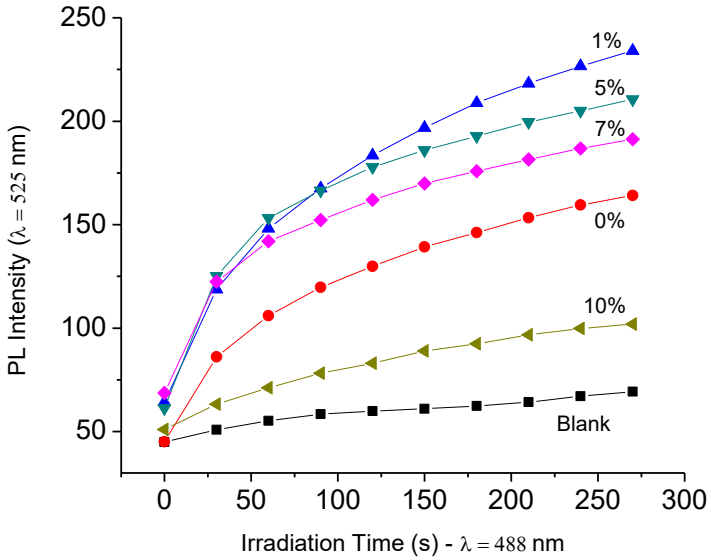

Figure 37 Increase of PL intensity of Singlet Oxygen with pure and Mg - doped ZnO nanoparticles as a function of the exposure time under UV light.

Is possible that sterilization of the samples under ultraviolet light would have promoted a pre-photo activation of the nanoparticles, which may have contributed to the generation of singlet oxygen and other reactive species that would explain the bactericidal capacity of zinc oxide.

4.1.6 Remarks

Pure and Mg doped ZnO nanoparticles were successfully synthesized via route polyol. The formation of desired structure was confirmed by X-Ray Diffraction and FT-IR spectroscopy techniques. The Mg doping do not affect the nanoparticles morphology. All the doped and pure nanoparticles exhibit strong UV and visible emission at room temperature. The nanoparticles exhibited bactericidal capacity against E. coli and it was dependent of dopant level and the nanoparticles concentration.

4.2 Chitosan/Cellulose blend films

4.2.1 Fourier Transform Infrared Spectroscopy

The results of the FT-IR spectra of the Chitosan/Cellulose blend films are shown in Figure 38. The band at 1651 cm^{-1} was assigned to the bending vibration of $–NH_2$ group in the chitosan structure, this band can also be attributed to absorbed water in the amorphous region or stretching vibration of C=O group [2][70]. Furthermore, the band at 3380 cm^{-1} is related to the stretching vibration of $-NH_2$ and -OH groups; these functional groups make possible the formation of homogeneous Chitosan/cellulose films [70].

The bands at 891 cm^{-1} and 1150 cm^{-1} are related to the antisymmetric stretching of the C-O-C bridge, this band were assigned to the skeleton of the chitosan and cellulose structure, likewise the bands at 1026 cm^{-1} and 1060 cm^{-1} correspond to stretching vibration of C-O-C from glycoside unit. The band at 2895 cm^{-1} is associate to stretching vibration of C-H in the glucose ring, the CH_2OH group, and the CH_3 in acetyl group. Other bands at 1377 cm^{-1}, 1411 cm^{-1}, and 1558 cm^{-1} can be assigned to bending vibration of

CH_3, C-H and N-H groups, respectively. The obtained information was in agreement with previous studies performed by X. Wang [2] and C. Stefanescu [70].

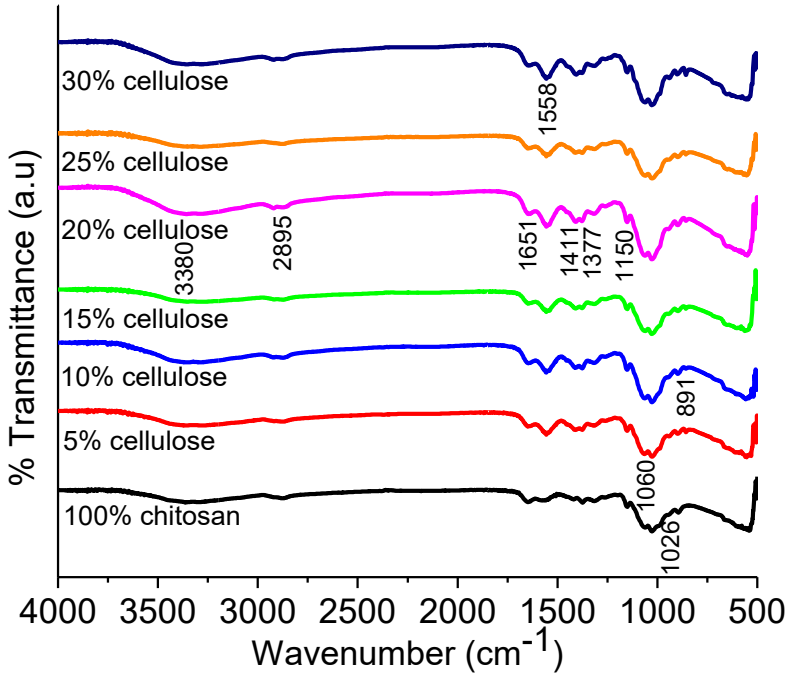

Figure 38 FTIR spectra of bare chitosan/cellulose film

4.2.2 Optical imaging

Optical microscope images of chitosan and chitosan/cellulose blend films are shown in Figure 39. The images revealed that the addition of cellulose appears to generate roughness in the films. Also we can see that there is a good dispersion of cellulose in the chitosan matrix, which indicates that there is a great compatibility between them, resulting in a homogeneous material.

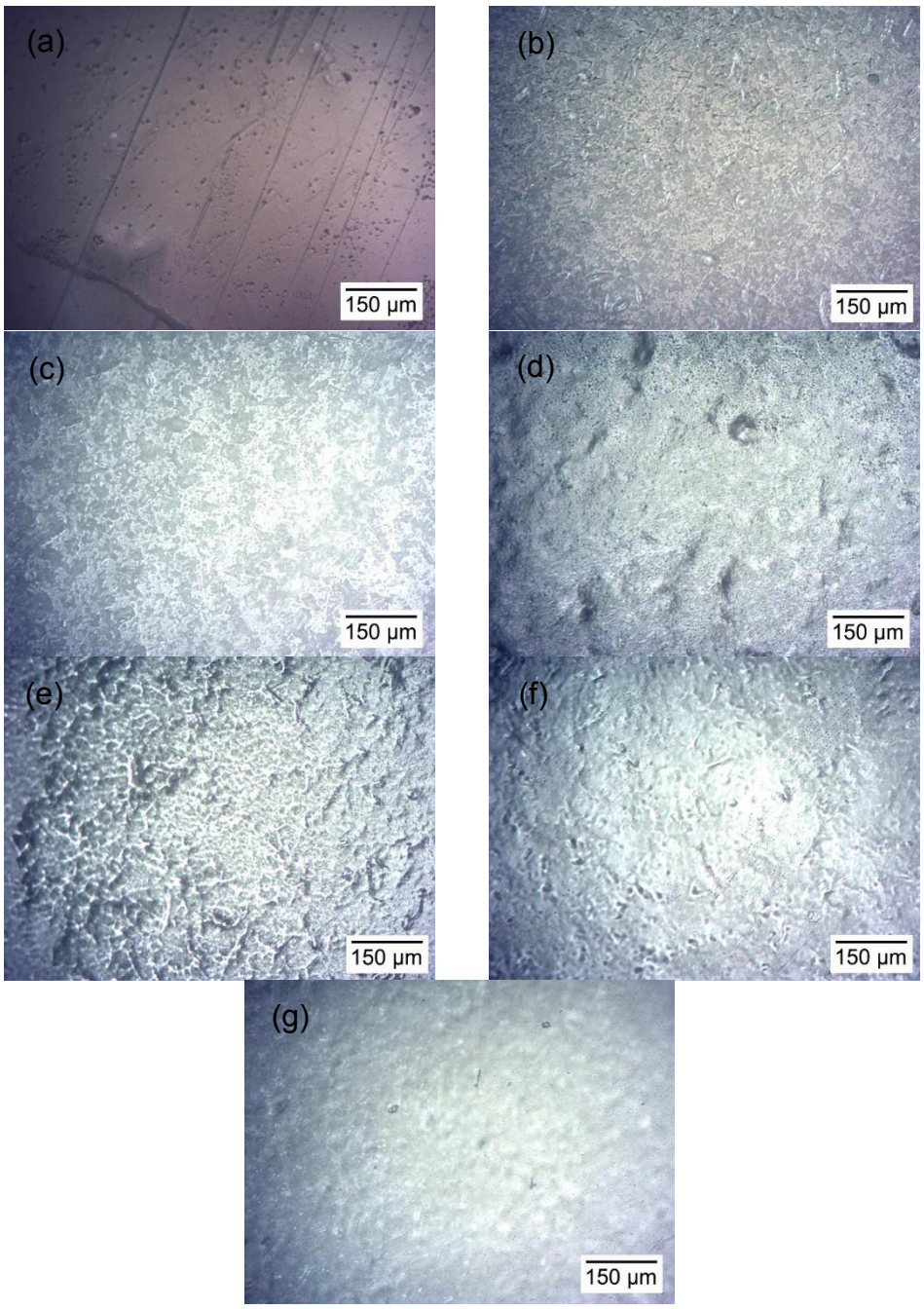

Figure 39 Optical images of chitosan and chitosan/cellulose blend films, (a) chitosan, (b) 5% cellulose, (c) 10% cellulose, (d) 15% cellulose, (e) 20% cellulose, (f) 25% cellulose and (g) 30% cellulose

4.2.3 Mechanical Properties

The Figure 40 shows a stress - strain curve of chitosan film, of this graph we can infer that the material has a brittle behavior, because no plastic zone is observed. The Ultimate Tensile Strength (UTS) and strain maxim calculated for this sample were 150 MPa and 3.97% respectively.

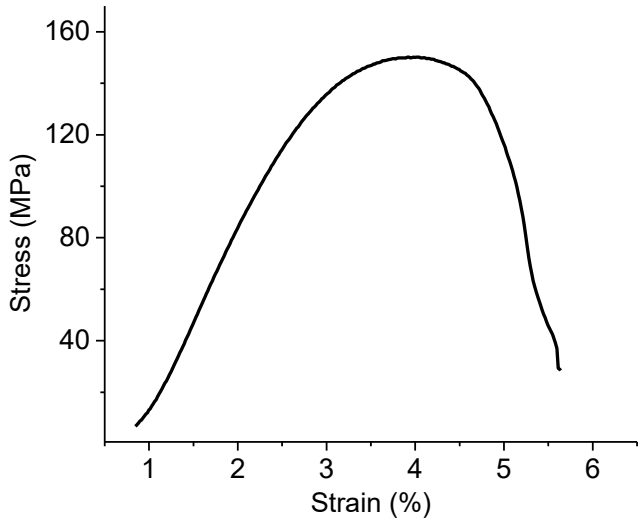

Figure 40 Stress – Strain curve of chitosan film

Cellulose was incorporated into the polymer matrix to different weight percent in order to increase the deformation of the material and determine a suitable condition. Figure 41 shows the representative stress - strain curves obtained of tension test carried out on the chitosan/cellulose films. The non-linear region, corresponding to the plastic deformation, evidenced the increase in the polymer ductility. This trend was observed in all films with exception of the one containing 30% cellulose.

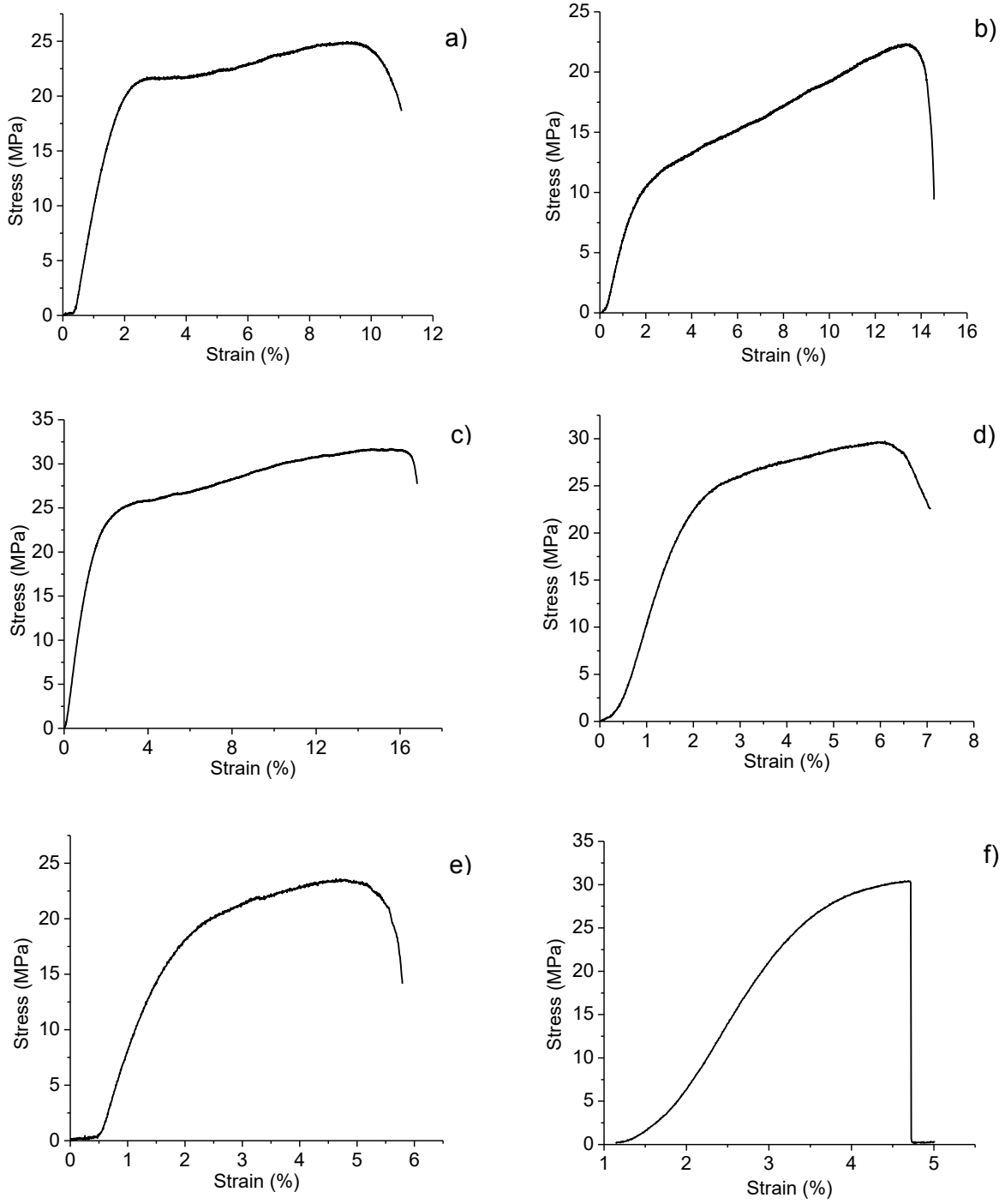

Figure 41 Stress – Strain curve of chitosan/cellulose films. a) 5% cellulose, b) 10% cellulose, c) 15% cellulose, d) 20 % cellulose, e) 25% cellulose and f) 30% cellulose

The variation of Ultimate Tensile Strength (UTS) and maximum strain with the addition of cellulose in the film is shown in Figure 42 and Figure 43, respectively. Figure 42 we can say that all the chitosan/cellulose films have a UTS lower than the chitosan film for which a value of 150 MPa was obtained. Likewise, in Figure 43 we can observe that the strain increases for all samples, reaching a maximum increase of 313.1%.

If we only use of Ultimate Tensile Strength of sample as criteria to decide which has better mechanical properties, should choose between those containing 15% and 30% of cellulose, but when comparing the strain percent of these samples, we determined that the film containing 15% cellulose has better mechanical properties.

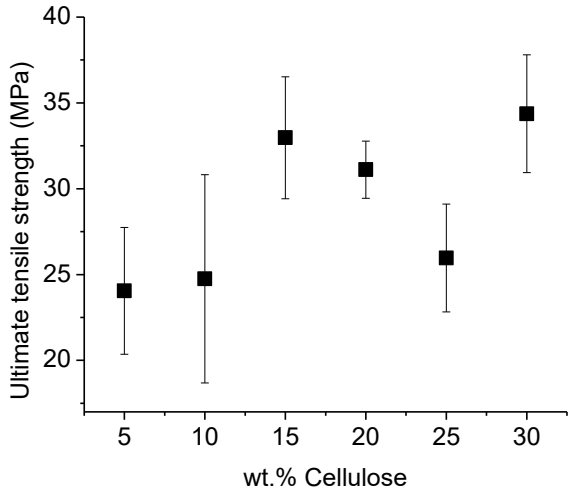

Figure 42 Measured Ultimate Tensile Strength of chitosan/cellulose/ Films

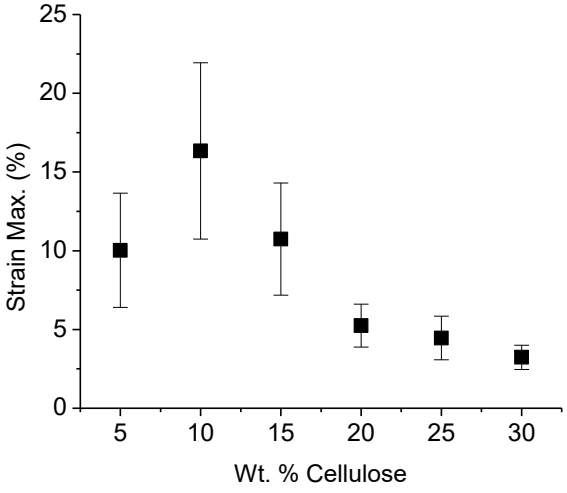

Figure 43 Measured strain maxim of chitosan/cellulose/ Films

4.2.4 Water vapor Permeability (WVP)

The water vapor permeability is an important property of packaging material that determines its application. The permeability consists of a solution - diffusion process, in our case is the ease with which the moisture penetrates in one side of the films and

diffuses to the other side. The values calculated for water vapor permeability of chitosan and chitosan/cellulose blend films are show in Figure 44. The values are in a range of 1.20 E^{-10} – 1.71 E^{-10} $gm^{-1}s^{-1}Pa^{-1}$.

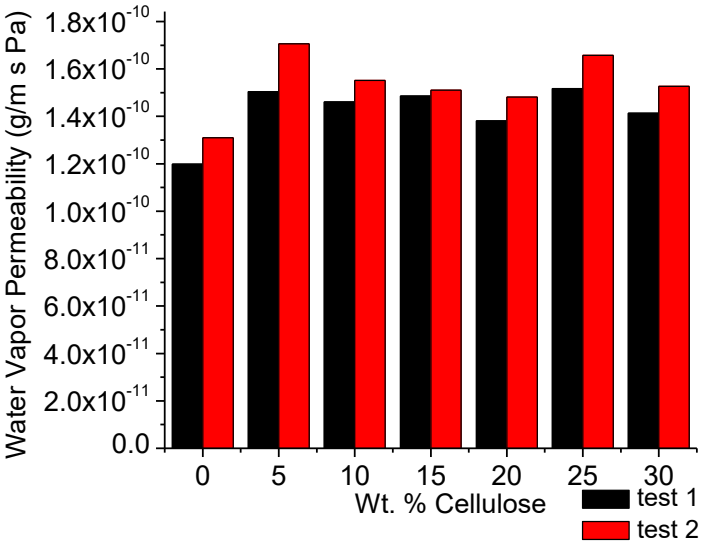

Figure 44 Water vapor Permeability of bare chitosan/cellulose blend film (duplicate tests)

In Figure 44, we can see that the addition of cellulose increases the permeability of the film, although this raise is not following a trend. Carrying out an ANOVA single factor, a P-value of 0.057 was determined Table 7. Therefore, we can say that the increase obtained in the permeability is not statistically significant.

Table 7 ANOVA single factor for Water vapor Permeability of bare chitosan/cellulose blend film

ANOVA

Source of Variation	*SS*	*df*	*MS*	*F*	*P-value*	*F crit*
Between Groups	0.163431	6	0.027239	3.659296	0.056834	3.865969
Within Groups	0.052106	7	0.007444			
Total	0.215537	13				

In contrast to synthetic polymers, films made with biopolymers have poor water barrier due to its hydrophilic nature, agree to this, our films showed high permeability. However, it is important to note that the chitosan / cellulose blend films showed a lower Water Vapor Permeability than some biopolymer films reported in the literature by Moura [47][71] and Padrao [72].

4.2.5 Remarks

Chitosan/cellulose blend films were successfully fabricated via solution casting. Morphological analysis revealed the formation of homogeneous films and an increase in the roughness of these. The tension test showed that the film with a cellulose content of 15% has better mechanical properties. Finally, we can say that the incorporation of cellulose had no significant effect on water permeability.

4.3 Chitosan/Cellulose Mg-ZnO nanocomposites

The film containing 85% chitosan and 15% cellulose was the polymeric matrix used to synthesize the nanocomposite bearing Mg (0.5 at.%)-ZnO as the disperse phase at different w/w loadings.

4.3.1 X-ray Diffraction Analyses

Figure 45 shows the XRD patterns of the Mg (0.5 at. %)-ZnO nanoparticles and the XRD of Chitosan/Cellulose films, with and without Mg-ZnO nanoparticles. The diffractogram for the Mg-ZnO powders shows the crystallographic planes corresponding to the ZnO-

wurtzite phase; the average crystallite size for this sample, calculated using the Scherrer's equation, was 7.2 ± 0.8 nm.

The spectra of chitosan/cellulose film exhibited two broad diffractions peaks centered on 2Θ=16.95° and 2Θ= 20° corresponding to the crystalline fraction of cellulose and chitosan respectively; the intense peak around 2Θ= 23° corresponds to cellulose [70][73].

The wurtzite diffraction peaks were not clearly identified in the nanocomposite pattern because of the small amount (10% w/w) of the oxide. Another possibility is that the nanoparticles are not in the surface of the composite and because of this could not be detected by the instrument.

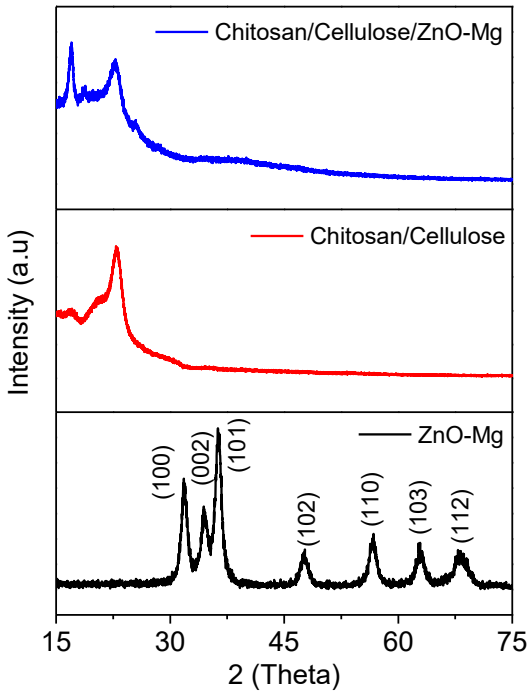

Figure 45 XRD patterns of bare chitosan/cellulose film, ZnO-Mg-bearing nanocomposite film and ZnO-Mg nanoparticles. 10% w/w was the nanoparticles loading in the nanocomposite

4.3.2 Fourier Transform Infrared Spectroscopy

The FTIR spectra of the Mg (0.5 at. %)- ZnO nanoparticles and the Chitosan/Cellulose films, with and without Mg-ZnO nanoparticles, are shown in Figure 46. The spectrum for Mg doped ZnO nanoparticles shows a clear band centered on 536 cm^{-1} that correspond to Zn-O stretching vibration [65]. The bands at 1072 cm^{-1} and 1420 cm^{-1} are associated to stretching vibration of -CO and bending vibration of -CH respectively these band reveal the presence of absorbed by product related to the functional groups of polyol. The band at 1595 cm^{-1} can be assigned to residual water on the surfaces of the samples. A band centered at 3381 cm^{-1} is attributed to O-H stretching vibration of hydroxyl group.

The FT-IR spectrum of the bare Chitosan/Cellulose blend film shows a band at 1651 cm^{-1} assigned to the bending vibration of $–NH_2$ group in the chitosan structure; the band at 3380 cm^{-1} is related to the stretching vibration of $-NH_2$ and -OH groups. The bands at 891 cm^{-1} and 1150 cm^{-1} are related to the antisymmetric stretching of the C-O-C bridge, assigned to the skeleton of the chitosan and cellulose structure, likewise the bands at 1026 cm^{-1} and 1060 cm^{-1} correspond to stretching vibration of C-O-C from glycoside unit. The band at 2895 cm^{-1} is associate to stretching vibration of C-H in the glucose ring, the CH_2OH group, and the CH_3 in acetyl group. Other bands at 1377 cm^{-1}, 1411 cm^{-1}, and 1558 cm^{-1} can be assigned to bending vibration of CH_3, C-H and N-H groups, respectively.

The spectrum of the chitosan/cellulose film containing 10% of Mg-doped ZnO nanoparticles did not exhibited a noticeable change in the characteristic bands, which may suggest that the nanoparticles addition did not affect the chemical structure of the polymer matrix. The spectrum obtained for the film containing 1%, 3% and 5% of Mg-

doped ZnO nanoparticles were similar to those for 10% w/w of loading. The characteristic band of ZnO (536 cm-1) was not observed due to its overlapping with chitosan/cellulose bands.

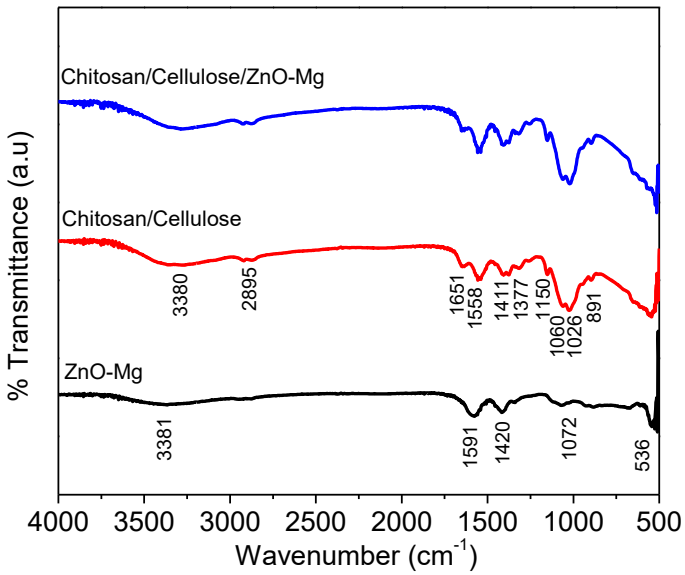

Figure 46 FTIR spectra of bare chitosan/cellulose film, ZnO-Mg-bearing nanocomposite film and ZnO-Mg nanoparticles.

4.3.3 Optical imaging

Nanocomposite surface was analyzed by optical microscopy in different areas of the sample. Images representative of bare chitosan/cellulose film and Mg-ZnO bearing nanocomposite film are shown in Figure 47. On a qualitative basis, the images revealed that the addition of ZnO-Mg nanoparticles induce roughness on the films. Also, the images evidenced a reasonably good dispersion of nanoparticles in the polymeric matrix because no large agglomerates were observed.

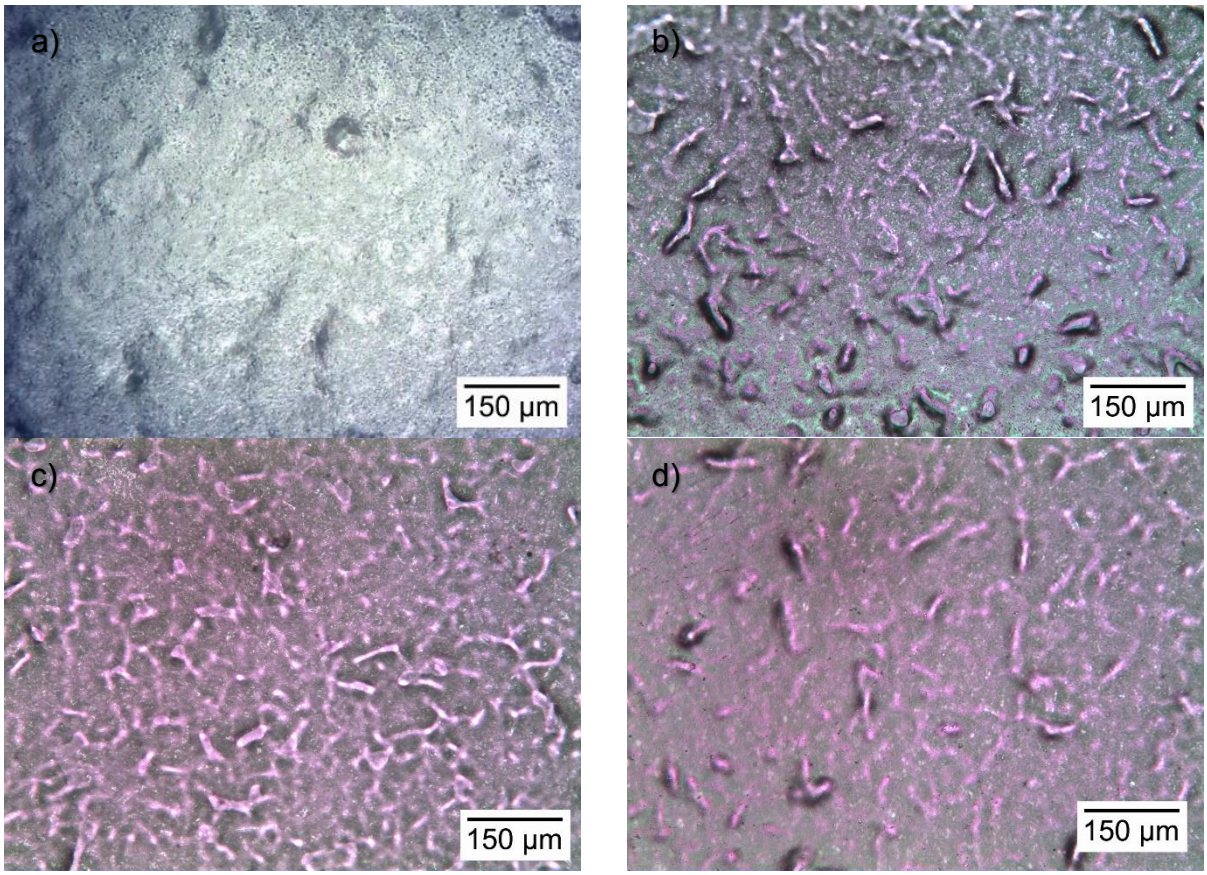

Figure 47 Optical images of chitosan/cellulose nanocomposite films containing a) 0%, b) 3%, c) 5% and d) 10% w/w ZnO-Mg nanoparticles.

4.3.4 Mechanical Properties of the Films

The variation of Ultimate Tensile Strength (UTS) and maximum strain of the films with the w/w loading of Mg-ZnO nanoparticles in the nanocomposite films are shown in Figure 48 and Figure 49, respectively. It is evident the strengthening of the corresponding films by importing Mg-ZnO dispersoids and the expected drop in maximum strain; these trends are attributed to the mechanical reinforcement of the soft polymeric matrix by embedded Mg-ZnO dispersoids. The proportional increase UTS regarding nanoparticles content also indicates a good dispersion of these dispersoids within the polymeric matrix.

When a product is handled, the packing material can be damaged as breakages and lacerations, generating losses of product content and more importantly, their ability to provide physical, chemical or biological protection is affected, leaving the product exposed to dust, insects or other factors and / or pollutants that contribute to the deterioration of this. In this regard, the determination of the mechanical properties is of considerable interest because it gives us an idea of the strength of the material to the manipulation.

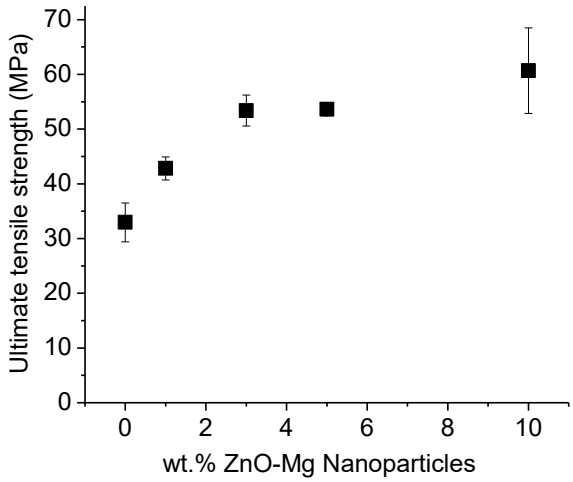

Figure 48 Ultimate Tensile Strength (MPa) of bare and Mg-ZnO bearing nanocomposite films

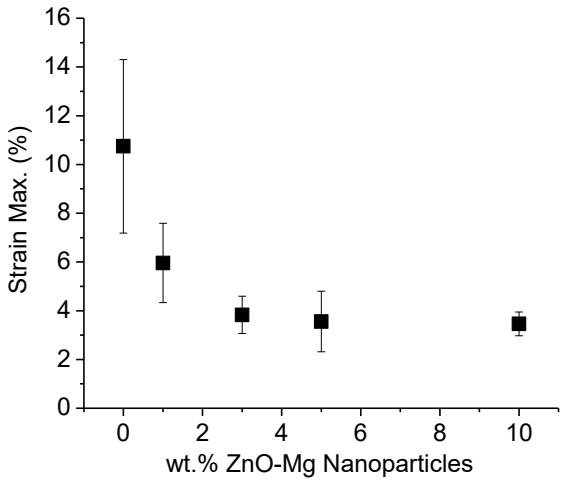

Figure 49 Maximum strain of bare and Mg-ZnO bearing nanocomposite films

4.3.5 Water Vapor Permeability

Figure 50 shows the values calculate for water vapor permeability of chitosan/cellulose/ZnO-Mg nanocomposites; this values are in a range of 1.49 E^{-10} - 1.82 E^{-10} $gm^{-1}s^{-1}Pa^{-1}$.

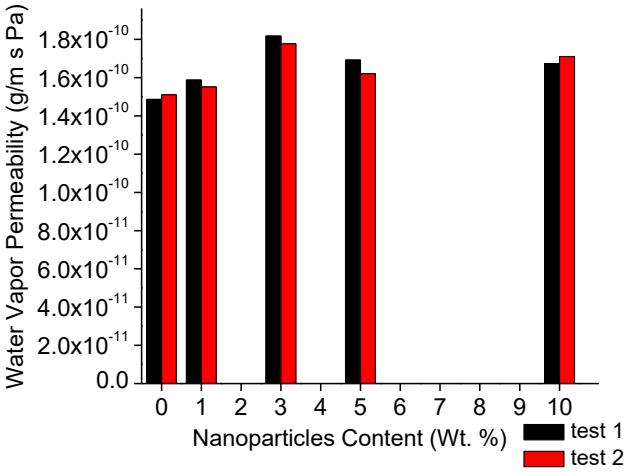

Figure 50 . Water Vapor Permeability of bare and Mg-ZnO-bearing nanocomposite film (duplicate tests)

The data in Figure 50 shows that the addition of nanoparticles increases the permeability of nanocomposites films, although this raise does not follow a clear a trend. Carrying out an ANOVA single factor, a P- Values of 0.002 was determined (Table 8). Therefore, we can say that the addition of nanoparticles has an effect statistically significant on the permeability.

Table 8 ANOVA single factor for Water vapor Permeability of chitosan/cellulose/ZnO-Mg nanocomposites

Source of Variation	***SS***	***df***	***MS***	***F***	***P-value***	***F crit***
Between Groups	0.1056	4	0.0264	26.1287	0.0012	5.1922
Within Groups	0.0050	5	0.0010			
Total	0.1106	9				

Studies report that the addition of nanoparticles decreases the permeability of the composites, because the nanoparticles prevent the diffusion of water molecules and these must move around the particle creating a diffusive tortuosity effect through the film [74][75].

In our case, the addition of nanoparticles increases the permeability, which can be explained considering the discontinuity generated by the nanoparticles in the material. In the work reported by Pelin Oymaci [75], describes that factors such as content, size and dispersion of the particle can affect the barrier properties, in this respect, the dispersion of the particles in the polymeric matrix is a critical factor, because the nanoparticles could generate discontinuity due to certain degree of agglomeration that would have the porosity.

The water vapor permeability is an important property of packaging material that determines its application. Each food product has its own requirements moisture level appropriate to maximize their shelf life during storage. Some food products such as fruits have biological activity during its storage generating gases and moisture. If moisture condenses on the product could accelerate the growth of molds and other post-harvest diseases. A material with a high water vapor permeability could offer solutions to this problem, in this sense, our material would have a possible application.

4.3.6 Bactericidal capacity against E. coli

Bactericidal capacity of the nanocomposite was evaluated by colony count method. The amount of nanocomposite in the culture medium was 0.015g, each nanocomposite was prepared with different amounts of nanoparticles, and therefore varied the amount of nanoparticle present in the culture medium, in Table 9 the bacterial inhibition obtained is reported for each nanocomposite.

Table 9 Bacterial inhibition percentage for E. coli

Nanoparticles in the nanocomposites (wt. %)	Equivalent in ppm	Bacterial inhibition (%)	Std Dev bacterial inhibition
0	0	-16.34	8.13
1	150	91.75	5.11
3	450	96.70	5.11
5	750	97.52	4.14
10	1500	96.70	2.56

Figure 51 shows the bacterial inhibition percentage for E. coli in presence of bare chitosan/cellulose film and Mg-ZnO nanocomposite film; all samples containing nanoparticles exhibited bactericidal effect.

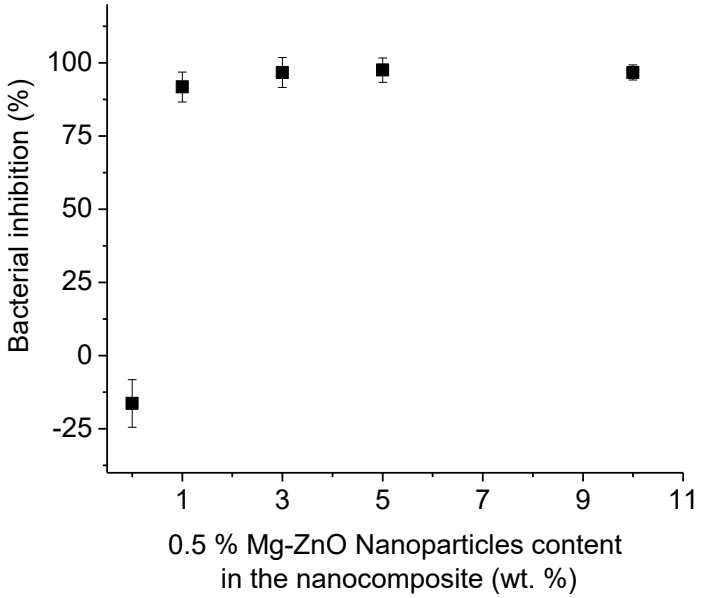

Figure 51 Bacterial inhibition percentage for E. coli in presence of: bare and Mg-ZnO bearing nanocomposite film. The bacteria were contacted with 0.015 g of nanocomposites cut into small pieces. The concentration of nanoparticles in the culture medium excluding the polymer matrix was 0, 150, 450, 750 and 1500 ppm.

Several mechanisms have been proposed to explain the antimicrobial properties of chitosan; the most accepted, provides that the amino group positively charged of chitosan interacts with the negatively charged of bacterial membrane affecting its permeability and generating leakage of intracellular material. In our case the chitosan/cellulose film does not show any bactericidal activity, which can be attributed to the content of cellulose present, Caro [74] reported that when combining chitosan with other polymers decreases its activity antimicrobial. The membrane containing no nanoparticles was a nutrient for bacteria whereby a negative value for the inhibition of growth was obtained.

On the contrary, as-synthesized nanocomposites exhibit a high antibacterial capacity, which can be attributed to the bactericidal effect of Mg-ZnO nanoparticles, where Mg species could have reinforced the bactericidal effect of pure ZnO. The involved mechanism was explained in section 4.1.5.

4.3.7 Remarks.

Chitosan/cellulose/ZnO-Mg nanocomposites films were successfully fabricated via solution casting. A structural analysis indicated that the nanoparticles addition did not affect the chemical structure of the polymeric matrix. An analysis of the film morphology revealed the formation of homogeneous films. The tension test showed that the addition of nanoparticles increases the UTS of the material while the deformation is reduced. Bactericidal assay reveals that all nanocomposites exhibited high bactericidal capacity against *E. coli* and this was not dependent on the amount of nanoparticle present in the matrix. Finally, we can say that the incorporation of ZnO-Mg nanoparticles increase the water vapor permeability.

5. General Conclusions

Pure and Mg doped ZnO nanoparticles were successfully synthesized via route polyol. The X- ray diffraction confirmed the formation of Zinc Oxide wurtzite- phase. The particles exhibited a strong violet emission that promote the formation of Zinc interstitials in the sample. The nanoparticles exhibited capacity of generate singlet oxygen and bactericidal effect against *E. coli*. The nanoparticle with doping level of Mg 0.5 at. % show the highest inhibition of bacterial growth, consequently this particle was inserted in the polymeric matrix.

Homogeneous Chitosan/cellulose blend films to different cellulose content were successfully fabricated via solution casting. The addition of cellulose increase the roughness and their water vapor permeability. Accordingly to mechanical properties we selected the film with a cellulose content of 15% like polymeric matrix to adding ZnO nanoparticles.

Finally, Homogeneous chitosan/cellulose ZnO-Mg nanocomposites were fabricated, the morphology analysis revealed a good dispersion of nanoparticles in the polymeric matrix, the FT-IR shows that the nanoparticles did not the affect the chemical structure however, a change in the mechanical properties can be appreciated in the tension test. Accordingly to bactericidal assays we can see that all nanocomposites has a high bactericidal capacity against *E. coli*.

References

[1] C.-M. Shih, Y.-T. Shieh, and Y.-K. Twu, “Preparation and characterization of cellulose/chitosan blend films,” *Carbohydr. Polym.*, vol. 78, no. 1, pp. 169–174, Aug. 2009.

[2] X. Wang, Y. Du, and H. Liu, “Preparation, characterization and antimicrobial activity of chitosan–Zn complex,” *Carbohydr. Polym.*, vol. 56, no. 1, pp. 21–26, May 2004.

[3] C. Stefanescu, W. H. Daly, and I. I. Negulescu, “Biocomposite films prepared from ionic liquid solutions of chitosan and cellulose,” *Carbohydr. Polym.*, vol. 87, no. 1, pp. 435–443, 2012.

[4] J. Iqbal, T. Jan, M. Ismail, N. Ahmad, A. Arif, and M. Khan, “In fl uence of Mg doping level on morphology , optical , electrical properties and antibacterial activity of ZnO nanostructures,” *Ceram. Int.*, vol. 40, no. 5, pp. 7487–7493, 2014.

[5] F. Liu, B. Qin, L. He, and R. Song, “Novel starch / chitosan blending membrane : Antibacterial , permeable and mechanical properties,” *Carbohydr. Polym.*, vol. 78, no. 1, pp. 146–150, 2009.

[6] A. Sorrentino, G. Gorrasi, and V. Vittoria, “Potential perspectives of bio-nanocomposites for food packaging applications,” *Trends Food Sci. Technol.*, vol. 18, no. 2, pp. 84–95, Feb. 2007.

[7] K. Vimala, Y. M. Mohan, K. S. Sivudu, K. Varaprasad, S. Ravindra, N. N. Reddy, Y. Padma, B. Sreedhar, and K. Mohanaraju, “Colloids and Surfaces B : Biointerfaces Fabrication of porous chitosan films impregnated with silver nanoparticles : A facile approach for superior antibacterial application,” vol. 76, pp. 248–258, 2010.

[8] A. Akbar and A. Kumar, “Zinc oxide nanoparticles loaded active packaging , a challenge study against Salmonella typhimurium and Staphylococcus aureus in ready- to-eat poultry meat,” *Food Control*, vol. 38, pp. 88–95, 2014.

[9] M. R. Ã, “Chitin and chitosan : Properties and applications,” vol. 31, pp. 603–632, 2006.

[10] M. Harfiz, E. Salleh, S. Nur, H. Mamat, A. Prof, and I. Idayu, “Starch Based Active Packaging Film Reinforced With Empty Fruit Bunch (EFB) Cellulose Nanofiber,” *Procedia Chem.*, vol. 9, pp. 23–33, 2014.

[11] H. V. Tran, L. D. Tran, C. T. Ba, H. D. Vu, T. N. Nguyen, D. G. Pham, and P. X. Nguyen, “Synthesis, characterization, antibacterial and antiproliferative activities

of monodisperse chitosan- based silver nanoparticles," *Colloids Surfaces A Physicochem. Eng. Asp.*, vol. 360, no. 1–3, pp. 32–40, May 2010.

[12] Y.-B. Wu, S.-H. Yu, F.-L. Mi, C.-W. Wu, S.-S. Shyu, C.-K. Peng, and A.-C. Chao, "Preparation and characterization on mechanical and antibacterial properties of chitsoan/cellulose blends," *Carbohydr. Polym.*, vol. 57, no. 4, pp. 435–440, Sep. 2004.

[13] R. Tankhiwale and S. K. Bajpai, "Colloids and Surfaces B : Biointerfaces Preparation , characterization and antibacterial applications of ZnO-nanoparticles coated polyethylene films for food packaging," *Colloids Surfaces B Biointerfaces*, vol. 90, pp. 16–20, 2012.

[14] V. K. Yemmireddy and Y.-C. Hung, "Selection of photocatalytic bactericidal titanium dioxide (TiO2) nanoparticles for food safety applications," *LWT - Food Sci. Technol.*, vol. 61, no. 1, pp. 1–6, Apr. 2015.

[15] D. Laha, A. Pramanik, A. Laskar, M. Jana, P. Pramanik, and P. Karmakar, "Shape-dependent bactericidal activity of copper oxide nanoparticle mediated by DNA and membrane damage," *Mater. Res. Bull.*, vol. 59, pp. 185–191, 2014.

[16] D. Sarkar, S. Tikku, V. Thapar, R. S. Srinivasa, and K. C. Khilar, "Formation of zinc oxide nanoparticles of different shapes in water-in-oil microemulsion," *Colloids Surfaces A Physicochem. Eng. Asp.*, vol. 381, no. 1–3, pp. 123–129, May 2011.

[17] M. G. Nair, M. Nirmala, K. Rekha, and A. Anukaliani, "Structural , optical , photo catalytic and antibacterial activity of ZnO and Co doped ZnO nanoparticles," *Mater. Lett.*, vol. 65, no. 12, pp. 1797–1800, 2011.

[18] Y. Xie, Y. He, P. L. Irwin, T. Jin, and X. Shi, "Antibacterial activity and mechanism of action of zinc oxide nanoparticles against Campylobacter jejuni.," *Appl. Environ. Microbiol.*, vol. 77, no. 7, pp. 2325–31, Apr. 2011.

[19] M. Vasanthi, K. Ravichandran, N. J. Begum, and G. Muruganantham, "Superlattices and Microstructures Influence of Sn doping level on antibacterial activity and certain physical properties of ZnO films deposited using a simplified spray pyrolysis technique," *Superlattices Microstruct.*, vol. 55, pp. 180–190, 2013.

[20] T. V Duncan, "Journal of Colloid and Interface Science Applications of nanotechnology in food packaging and food safety : Barrier materials , antimicrobials and sensors," *J. Colloid Interface Sci.*, vol. 363, no. 1, pp. 1–24, 2014.

[21] J. Lu and M. Bowles, "How Will Nanotechnology Affect Agricultural Supply Chains ?," vol. 16, no. 2, pp. 21–42, 2013.

[22] A. Moezzi, A. M. Mcdonagh, and M. B. Cortie, “Zinc oxide particles : Synthesis , properties and applications,” *Chem. Eng. J.*, vol. 185–186, pp. 1–22, 2012.

[23] A. F. Hepp, “One dimensional-ZnO nanostructures : synthesis , properties and environmental applications . Mater Sci Semicond Process,” no. July 2016, 2013.

[24] RAMÓN TENA ZAERA UNIVERSITAT DE VALENCIA, “El óxido de zinc: crecimiento cristalino mediante transporte en fase gaseosa y caracterización de propiedades físicas.,” universidad de valencia, 2004.

[25] A. Onodera and M. Takesada, “Electronic Ferroelectricity in II-VI Semiconductor ZnO.”

[26] A. M. Wesche, J. B. Gurtler, B. P. Marks, and E. T. Ryser, “Stress , Sublethal Injury , Resuscitation , and Virulence of Bacterial Foodborne Pathogens †,” vol. 72, no. 5, pp. 1121–1138, 2009.

[27] Y. Xie, Y. He, P. L. Irwin, T. Jin, Y. Xie, Y. He, P. L. Irwin, T. Jin, and X. Shi, “Antibacterial Activity and Mechanism of Action of Zinc Oxide Nanoparticles against Campylobacter jejuni Antibacterial Activity and Mechanism of Action of Zinc Oxide Nanoparticles against Campylobacter jejuni □,” 2011.

[28] H. Ma, P. L. Williams, and S. A. Diamond, “Ecotoxicity of manufactured ZnO nanoparticles e A review,” *Environ. Pollut.*, vol. 172, pp. 76–85, 2013.

[29] M. Mirhosseini and M. Afzali, “Investigation into the antibacterial behavior of suspensions of magnesium oxide nanoparticles in combination with nisin and heat against Escherichia coli and Staphylococcus aureus in milk,” vol. 68, pp. 208–215, 2016.

[30] A. Bhatnagar and M. Sillanpää, “Applications of chitin- and chitosan-derivatives for the detoxi fi cation of water and wastewater — A short review,” *Adv. Colloid Interface Sci.*, vol. 152, no. 1–2, pp. 26–38, 2009.

[31] C. K. S. Pillai, W. Paul, and C. P. Sharma, “Progress in Polymer Science Chitin and chitosan polymers : Chemistry , solubility and fiber formation,” vol. 34, pp. 641–678, 2009.

[32] V. K. Mourya and N. N. Inamdar, “Reactive & Functional Polymers Chitosan-modifications and applications : Opportunities galore,” vol. 68, pp. 1013–1051, 2008.

[33] P. K. Dutta, J. Dutta, and V. S. Tripathi, “Chitin and chitosan : Chemistry , properties and applications,” vol. 63, no. January, pp. 20–31, 2004.

[34] P. K. Dutta, S. Tripathi, G. K. Mehrotra, and J. Dutta, “Perspectives for chitosan based antimicrobial films in food applications,” *Food Chem.*, vol. 114, no. 4, pp. 1173–1182, 2009.

[35] D. Raabe, C. Sachs, and P. Romano, “The crustacean exoskeleton as an example of a structurally and mechanically graded biological nanocomposite material,” vol. 53, pp. 4281–4292, 2005.

[36] V. Zargar, M. Asghari, and A. Dashti, “A Review on Chitin and Chitosan Polymers : Structure , Chemistry , Solubility , Derivatives , and Applications,” no. 3, pp. 204–226, 2015.

[37] M. Royo and J. I. Mate, “Food Hydrocolloids Antifungal activity of films and solutions based on chitosan against typical seed fungi,” vol. 23, pp. 2309–2314, 2009.

[38] I. A. Alsarra, “International Journal of Biological Macromolecules Chitosan topical gel formulation in the management of burn wounds,” vol. 45, pp. 16–21, 2009.

[39] V. M. Esquerdo, T. R. S. C. Jr, G. L. Dotto, and L. A. A. Pinto, “Journal of Colloid and Interface Science Chitosan scaffold as an alternative adsorbent for the removal of hazardous food dyes from aqueous solutions,” *J. Colloid Interface Sci.*, vol. 424, pp. 7–15, 2014.

[40] M. Hosseinnejad and S. Mahdi, “International Journal of Biological Macromolecules Evaluation of different factors affecting antimicrobial properties of chitosan,” *Int. J. Biol. Macromol.*, vol. 85, pp. 467–475, 2016.

[41] M. T. Madigan, S. I. U. Carbondale, J. M. Martinko, S. I. U. Carbondale, D. A. Stahl, U. of W. Seattle, D. P. Clark, and S. I. U. Carbondale, *Biology of Microorganisms*, Thirteenth. 2011.

[42] S. Ummartyotin and H. Manuspiya, “A critical review on cellulose : From fundamental to an approach on sensor technology,” *Renew. Sustain. Energy Rev.*, vol. 41, pp. 402–412, 2015.

[43] G. Siqueira, J. Bras, and A. Dufresne, “Cellulosic Bionanocomposites: A Review of Preparation, Properties and Applications,” no. i, pp. 728–765, 2010.

[44] X. Luo and L. Zhang, “New solvents and functional materials prepared from cellulose solutions in alkali / urea aqueous system,” *FRIN*, 2010.

[45] S. Hokkanen and A. Bhatnagar, “A review on modi fi cation methods to cellulose-based adsorbents to improve adsorption capacity,” vol. 91, pp. 156–173, 2016.

[46] B. Mathew, A. Lopes, S. Ferreira, D. Souza, L. Maria, M. Costa, G. Molina, D. Olyveira, M. Kottaisamy, E. R. Nagarajan, and S. Thomas, “Cellulose nanocomposites with nanofibres isolated from pineapple leaf fibers for medical applications,” *Carbohydr. Polym.*, vol. 86, no. 4, pp. 1790–1798, 2011.

[47] M. R. De Moura, R. J. Avena-bustillos, T. H. Mchugh, D. F. Wood, C. G. Otoni, and L. H. C. Mattoso, “Miniaturization of cellulose fibers and effect of addition on the mechanical and barrier properties of hydroxypropyl methylcellulose films,” vol. 104, pp. 154–160, 2011.

[48] Alexander W. Chin, “Polymers for Innovative Food Packaging,” 2010.

[49] “CUALIDADES DE LOS MATERIALES PLÁSTICOS.” [Online]. Available: http://www.eis.uva.es/~macromol/curso11-12/Gema/envases-y-embalajes/pagina204.html.

[50] V. Gomes, L. Souza, and A. L. Fernando, “Nanoparticles in food packaging : Biodegradability and potential migration to food — A review,” *Food Packag. Shelf Life*, vol. 8, pp. 63–70, 2016.

[51] S. H. Othman, “Bio-nanocomposite Materials for Food Packaging Applications : Types of Biopolymer and Nano-sized Filler,” *Ital. Oral Surg.*, vol. 2, pp. 296–303, 2014.

[52] Food and drug Administration, “Bacteriological Analytical Manual Chapter 4,” 2002. [Online]. Available: http://www.fda.gov/Food/FoodScienceResearch/LaboratoryMethods/ucm064948.htm.

[53] Centers for Disease Control and Prevention, “E. coli,” 2015. [Online]. Available: http://www.cdc.gov/ecoli/).

[54] J. B. Gurtler, R. B. Bailey, D. J. Geveke, and H. Q. Zhang, “Pulsed electric fi eld inactivation of E . coli O157 : H7 and non-pathogenic surrogate E . coli in strawberry juice as in fl uenced by sodium benzoate , potassium sorbate , and citric acid q,” vol. 22, pp. 1689–1694, 2011.

[55] M. Vafaee and M. S. Ghamsari, “Preparation and characterization of ZnO nanoparticles by a novel sol – gel route,” vol. 61, pp. 3265–3268, 2007.

[56] A. Pinotti, M. A. Garcı, M. N. Martino, and N. E. Zaritzky, “ARTICLE IN PRESS Study on microstructure and physical properties of composite films based on chitosan and methylcellulose,” vol. 21, pp. 66–72, 2007.

[57] Y. Collantes and O. Perales-perez, “Effect of Crystal Size on the Structural and Functional Properties of Water- Stable Monodisperse ZnO Nanoparticles Synthesized Via a Polyol-Route,” pp. 1–6.

[58] Melina Pérez-Altamar and Oscar Perales-Pérez, “Fabrication and Characterization of Chitosan/Cellulose-ZnO Nanocomposites for Bactericidal Applications,” vol. 1685, pp. 1–6, 2014.

[59] Melina Perez-Altamar, Hilary Marrero, Milton Martinez and Oscar Peralez-Pérez “Study of Bactericidal Properties of Mg-Doped ZnO Nanoparticles,” *MRS Proc.*, vol. 1804, pp. 31–36, 2015.

[60] Barbara L Dutrow Louisiana State University and E. M. U. , Christine M. Clark, “No Title,” *X-ray Powder Diffraction (XRD)*. [Online]. Available: http://serc.carleton.edu/research_education/geochemsheets/techniques/XRD.html.

[61] Phil Jeffrey, “No Title,” *X-ray Data Collection Course*, 2006. [Online]. Available: http://xray0.princeton.edu/~phil/Facility/Guides/XrayDataCollection.html.

[62] instron, “Tensile Testing.” [Online]. Available: http://www.instron.us/en-us/our-company/library/test-types/tensile-test.

[63] Milton Martinez Julca, “Effect of the Incorporation of Defects in ZnO Nanocrystals on the Generation of Reactive Oxygen Species for Applications in Photodynamic Therapy,” M.S. thesis, Dept. Physics, University of Puerto Rico, Mayagüez, Puerto Rico, 2015.

[64] Y. Collantes Goicochea, “Synthesis and Characterization of ZnO-based Nanostructures for Potential Biomedical Applications,” M.S. thesis, Dept. Physics, University of Puerto Rico, Mayagüez, Puerto Rico, 2013.

[65] R. C. Pawar, J. S. Shaikh, P. S. Shewale, and P. S. Patil, “Characterization of zinc oxide nanoparticles synthesized by polymer assisted deposition method,” *J. Alloys Compd.*, vol. 509, no. 5, pp. 1716–1721, 2011.

[66] N. Talebian, S. Matin, and M. Doudi, “Journal of Photochemistry and Photobiology B : Biology Controllable synthesis of ZnO nanoparticles and their morphology-dependent antibacterial and optical properties,” *J. Photochem. Photobiol. B Biol.*, vol. 120, pp. 66–73, 2013.

[67] M. D. Sanchez-garcia and J. M. Lagaron, “Natural micro and nanobiocomposites with enhanced barrier properties and novel functionalities for food biopackaging applications,” *Trends Food Sci. Technol.*, vol. 21, no. 11, pp. 528–536, 2010.

[68] M. Ramani, S. Ponnusamy, and C. Muthamizhchelvan, “Zinc oxide nanoparticles : A study of defect level blue – green emission,” *Opt. Mater. (Amst).*, vol. 34, no. 5, pp. 817–820, 2012.

[69] Y. Cedeño-Mattei, R. Concepción-Abreu and Oscar Perales-Pérez. Synthesis of ZnxMg1-xO Nanocrystals and the Assessment of their Antimicrobial Activity against Escherichia Coli. vol. 1675, 2014.

[70] C. Stefanescu, W. H. Daly, and I. I. Negulescu, “Biocomposite films prepared from ionic liquid solutions of chitosan and cellulose,” *Carbohydr. Polym.*, vol. 87, no. 1, pp. 435–443, Jan. 2012.

[71] M. R. De Moura, L. H. C. Mattoso, and V. Zucolotto, “Development of cellulose-based bactericidal nanocomposites containing silver nanoparticles and their use as active food packaging,” vol. 109, pp. 520–524, 2012.

[72] S. Gonçalves, P. Silva, V. Sencadas, J. Padr, A. C. Pinheiro, and F. Dourado, “Food Hydrocolloids Bacterial cellulose-lactoferrin as an antimicrobial edible packaging,” vol. 58, pp. 126–140, 2016.

[73] S. Li, N. Jia, J. Zhu, M. Ma, F. Xu, B. Wang, and R. Sun, “Rapid microwave-assisted preparation and characterization of cellulose – silver nanocomposites,” *Carbohydr. Polym.*, vol. 83, no. 2, pp. 422–429, 2011.

[74] L. Abugoch, N. Caro, E. Medina, M. Díaz-dosque, L. Luis, and C. Tapia, “Food Hydrocolloids Novel active packaging based on fi lms of chitosan and chitosan / quinoa protein printed with chitosan-tripolyphosphate-thymol nanoparticles via thermal ink-jet printing,” vol. 52, pp. 520–532, 2016.

[75] P. Oymaci and S. Alsoy, “Food Hydrocolloids Improvement of barrier and mechanical properties of whey protein isolate based food packaging fi lms by incorporation of zein nanoparticles as a novel bionanocomposite,” *Food Hydrocoll.*, vol. 54, pp. 1–9, 2016.